haematologica
Journal of the Ferrata Storti Foundation

# Different primary thyroid B-cell lymphomas show overlapping mutation profiles, suggesting involvement of a common pathogenic process

*by Maria-Myrsini Tzioni, Natsuko Watanabe, Ellen Stelloo, Zi Chen, Adheesh Ghosh, Fangtian Wu, Kiminori Sugino, Koichi Ito, Harma Feitsma, Manabu Fujisawa, Mamiko Sakata-Yanagimoto, Lìvia Rásó-Barnett, Teresa Marafioti, Ayoma D. Attygalle, Andrew Wotherspoon and Ming-Qing Du*

*Received: May 28, 2025.*
*Accepted: March 6, 2026.*

*Citation: Maria-Myrsini Tzioni, Natsuko Watanabe, Ellen Stelloo, Zi Chen, Adheesh Ghosh, Fangtian Wu, Kiminori Sugino, Koichi Ito, Harma Feitsma, Manabu Fujisawa, Mamiko Sakata-Yanagimoto, Lìvia Rásó-Barnett, Teresa Marafioti, Ayoma D. Attygalle, Andrew Wotherspoon and Ming-Qing Du. Different primary thyroid B-cell lymphomas show overlapping mutation profiles, suggesting involvement of a common pathogenic process.*
*Haematologica. 2026 Mar 19. doi: 10.3324/haematol.2025.288239 [Epub ahead of print]*

**Different primary thyroid B-cell lymphomas show overlapping mutation profiles, suggesting involvement of a common pathogenic process**

Maria-Myrsini Tzioni[1], Natsuko Watanabe[2], Ellen Stelloo[3], Zi Chen[1], Adheesh Ghosh[4], Fangtian Wu[1], Kiminori Sugino[5], Koichi Ito[5], Harma Feitsma[3], Manabu Fujisawa[6,7], Mamiko Sakata-Yanagimoto[6,8,9], Lívia Rásó-Barnett[10], Teresa Marafioti[4,11], Ayoma D Attygalle[12], Andrew Wotherspoon[12], Ming-Qing Du[1]

[1]Department of Pathology, University of Cambridge, Cambridge, UK;

[2]Department of Internal Medicine, Ito Hospital, Tokyo, Japan;

[3]Cergentis BV, Utrecht, Netherlands;

[4]Cancer Institute, University College London, London, United Kingdom.

[5]Department of Surgery, Ito Hospital, Tokyo, Japan;

[6]Department of Hematology, Institute of Medicine, University of Tsukuba, Ibaraki, Japan;

[7]Centre for Lymphoid Cancer department, BC Cancer, Vancouver, British Columbia, Canada;

[8]Department of Hematology, University of Tsukuba Hospital, Ibaraki, Japan;

[9]Division of Advanced Hemato-Oncology, Transborder Medical Research Center, University of Tsukuba, Ibaraki, Japan;

[10]The Haematopathology and Oncology Diagnostic Service, Addenbrookes Hospital, Cambridge, UK;

[11]Department of Cellular Pathology, University College London Hospitals NHS Foundation Trust, London, United Kingdom.

[12]Department of Histopathology, The Royal Marsden Hospital, London, UK;

**Running title**: Mutation profile of thyroid lymphoma

**Key words**: thyroid lymphoma, mutation profile, chromosome translocation, autoimmunity, histopathology

Correspondence to

Professor Ming-Qing Du,

Division of Cellular and Molecular Pathology,

Department of Pathology, University of Cambridge

Box 231, Level 3, Lab Block, Addenbrooke's Hospital,

Hills Road, Cambridge, CB2 2QQ, United Kingdom

Tel: +44 (0)1223 767092; Fax: +44 (0)1223 586670; Email: mqd20@cam.ac.uk

**Data-sharing statement:** All core data generated or analysed during this study are included in this published article, and additional raw data are available from the corresponding author on reasonable request.

**Acknowledgements:** The authors would like to thank Dr Ana Toribio and Jessica Ferreira Gouveia for their assistance with Illumina sequencing.

**Authors contributions:** FISH, targeted NGS, data collection and analyses: MMT, ES, ZC, FW, AG, TM, MQD; Mouse experimental data: MF & MSY; Case contribution and pathology: NW, KS, KI, LRB, ADA, AW, MQD; Study conception, coordination and research funding: MQD, NW; Manuscript writing and preparation: MQD & MMT with contributions from all authors. All authors read and approved the final manuscript.

**Conflict of interest:** Ellen Stelloo and Harma Feitsma are employees of Cergentis BV, the company that developed the Targeted Locus Capture (TLC) technology used in this study. The other authors declare no competing financial or non-financial interests.

**Sources of Research support:** The study was supported by research grants from Blood Cancer UK (22011, 24011, 19011, 19010), Cancer Research UK (CRCBPA-Nov23/100001, C8333/A29707) and an International Collaborative Award from the Pathological Society of Great Britain and Ireland, UK (ICA 1019 01). MMT was supported by a BBSRC DTP PhD studentship (BBSRC BB/M011194/1). MF was supported by Gilead's Research Scholars Program and The Leukemia & Lymphoma Society (3442-25). The Human Research Tissue Bank of the Cambridge University Hospitals NHS Foundation Trust is supported by the NIHR Cambridge Biomedical Research Centre.

**ABSTRACT**

Primary thyroid lymphomas commonly originate from a background of Hashimoto's thyroiditis and comprise largely extranodal marginal zone lymphoma of mucosa-associated lymphoid tissue (EMZL), diffuse large B-cell lymphoma (DLBCL), and follicular lymphoma (FL). Thyroid EMZL harbours a distinct mutation profile, but whether this discriminates them from thyroid FL and DLBCL is unknown. To investigate this, we have investigated 42 EMZL (11 *BCL6*-tr+ve), 21 FL (5 *BCL2*-tr+ve, 10 *BCL6*-tr+ve, 1 both *BCL2/BCL6*-tr+ve) and 34 DLBCL of the thyroid. Targeted NGS revealed a remarkable overlap in the mutation profile among thyroid EMZL, *BCL2*-tr-ve FL and DLBCL, all showing frequent mutations in *TET2*, *IGLL5, TNFRSF14, CD274, GNA13, FAS, KLF2* and *TNFAIP3*. In contrast, *BCL2*-tr+ve FL of the thyroid showed frequent *BCL2*, *KMT2D*, *CREBBP*, *EZH2*, but not *TET2* and *CD274* mutations. Genomic analysis of *BCL6* translocation by targeted locus capture NGS showed different genomic configurations between thyroid FL and EMZL. In thyroid FL, majority of *BCL6* translocations placed its coding exons under the transcriptional control of the *IGH* switch region super-enhancer or its partner genes, potentially resulting in *BCL6* constitutive expression. In contrast, majority of *BCL6* translocations in thyroid EMZL juxtaposed the *BCL6* gene to the IGHJ/D region without encompassing the Eμ enhancer or its partner genes in an opposite orientation, thus less likely to lead to constitutive *BCL6* transactivation. The above genetic changes likely dysregulate B-cell maturation and peripheral tolerance, thus offer significant molecular insights into the pathogenesis of thyroid lymphomas, particularly underpinning autoimmunity in the lymphomagenesis and potentially explaining the overlap in histopathology between EMZL and FL.

## INTRODUCTION

Primary thyroid lymphomas commonly originate from a background of chronic lymphocytic thyroiditis (Hashimoto's thyroiditis, HT) and comprise largely extranodal marginal zone lymphoma of mucosa-associated lymphoid tissue (EMZL), diffuse large B-cell lymphoma (DLBCL), and followed by follicular lymphoma (FL) [1]. The histological diagnosis of these thyroid lymphomas can be readily made by integrated histological and immunophenotypic assessment in most cases. However, a high proportion of thyroid FL are negative for *BCL2* translocation and lack expression of CD10. These cases often pose significant difficulty in differential diagnosis from thyroid EMZL that frequently show prominent follicular colonisation, hence considerable overlap in their morphological and immunophenotypic presentations [2].

We previously showed that thyroid EMZL had a distinct mutation profile characterised by concurrent mutations in *TET2*, *CD274* (PD-L1) and *TNFRSF14*, distinguishing them from those of other B-cell lymphomas including EMZL at other anatomic sites [3–5]. However, the genetic profile of thyroid FL and DLBCL remains to be unravelled, particularly whether there is any difference in the genetic profile between thyroid FL and EMZL, if so whether such genetic differences can help their differential diagnosis. In addition, *BCL6* translocation is occasionally seen in EMZL, but seemingly more frequent in those of the thyroid [6–8]. This is rather paradoxical given that BCL6 functions as a master regulator of the germinal centre (GC) reaction, preventing GC B-cell exit by repressing the plasma cell differentiation programme [9,10]. To address these questions and further understand the pathogenesis of thyroid lymphomas, we performed targeted next generation sequencing (NGS) of 172 lymphoma genes and integrated analyses in a large cohort of primary thyroid lymphoma including 42 EMZL, 21 FL and 34 DLBCL. We also investigated the genomic configuration of *BCL6* translocation in thyroid FL and EMZL by targeted locus capture NGS in order to understand the paradoxical finding of *BCL6* translocation in thyroid EMZL.

## METHODS

### Patients and clinical data

The use of archival tissues for research was approved by the ethics committees of the involved institutions.

A total of 97 cases of primary thyroid B-cell lymphoma (94 from Ito Hospital, Tokyo) were successfully investigated, including 24 cases of EMZL subjected to a previous study [3]. The histological diagnosis was reviewed with the help of additional immunohistochemistry (Table S1) and interphase fluorescence *in situ* hybridisation for *BCL2* and *BCL6* translocations by expert haematopathologists (AW, ADA). The final diagnosis compromised 42 EMZL (11 with *BCL6* translocation), 21 FL (5 with *BCL2* translocation, 10 with *BCL6* translocation, 1 case with both *BCL2* and *BCL6* translocations, 5 lacking both *BCL2* and *BCL6* translocations) and 34 DLBCL (Table S4).

### DNA extraction and quality assessment

In each case, tumour rich areas (>30%) were microdissected on formalin-fixed paraffin-embedded (FFPE) tissue slides. DNA was extracted and assessed for quality by PCR of variably sized genomic fragments as previously described [11].

### Mutation analysis by targeted next generation sequencing

The target panel included 172 genes recurrently mutated in MZL, FL and DLBCL (Table S2). FFPE tissue DNA (100ng) were fragmented using the Covaris E220 Focused Ultrasonicator (Covaris, Brighton, UK). For each DNA sample, an indexed library was prepared using the xGen™ UDI-UMI

indexes (IDT, Coralville, IA, USA), and pooled for target enrichment using TWIST probes (TWIST Biosciences, San Francisco, CA, USA). The enriched DNA targets were amplified by PCR and then pooled together for sequencing using the Illumina NextSeq 2000 platform (2x100bp paired-end sequencing protocol). The sequence data analysis, variant calling, and filtering were performed as described in our previous studies [12,13].

For DNA sample with suboptimal quality (PCR amplification of genomic fragment ≤300bp), targeted sequencing was performed in duplicate and only variants detected by both replicates were considered as a true change (Figure S1).

**Mutation signature analysis**

This analysis was based on all somatic single base substitutions including synonymous, non-synonymous, splice site and UTR changes using Sigprofiler assignment [14].

**Genomic analysis of chromosome translocation by next generation sequencing**

The genomic configuration of *BCL6* translocation was investigated by targeted locus capture next generation sequencing (TLC-NGS) as described previously and a customised NGS panel (Supplementary methods) [15]. The *IGH* genomic segments including super enhancer positions were according to those described previously using the hg19 assembly [16].

**Re-analysis of single-cell RNA-sequencing data from mice germinal centre B cells**

*TET2* inactivation by mutation may cause genome-wide hypermethylation, hence potentially impact on gene expression in B cells and their phenotype. To explore this, we revisited the single cell sequencing data from a previous mouse study [17].

GC B cells sorted from the spleens of tumor-bearing Tet2-deficient (MxTR) and wild-type (MxWT) mice were used for library preparation for RNA sequencing (RNA-seq: MxRT, n=5; MxWT, n=4) and whole-genome bisulfite sequencing (WGBS: MxTR, n=2; MxWT, n=2). Sequencing data was reanalysed as previously described [17]. Differential expression data from RNA-seq were analysed using DESeq2 [18]. The methylation rate of each base by WGBS was visualised in the UCSC Genome Browser.

**Statistical analysis**

The comparison of mutation load and gene expression among different groups was assessed using Wilcoxon Rank-Sum test with two-sided P values. Association between mutation frequencies and clinical parameters among lymphoma groups and their subsets was examined using the Fisher's exact test. Mutation association was analysed using the somaticInteractions function in the Maftools R Bioconductor package [19].

**RESULTS**

**Histopathological and immunophenotypic features of thyroid lymphoma**

In comparison with EMZL of other sites, thyroid cases showed prominent follicular colonisations albeit variable extent in cases. Among the 40 cases of thyroid EMZL with complete CD21, CD10 and BCL6 immunohistochemistry data, 38 showed extensive follicular colonisation, predominantly type 1 (poorly defined follicle/mantle zone) or type 2 (follicle and mantle zone variably preserved) pattern in 24 and 14 cases respectively [20]. Irrespective of different follicular colonisation patterns, 30 cases showed virtually absent CD10 expression in all or most colonised follicles, albeit variable BCL6

staining (Figure 1). The remaining 8 cases showed a mixed pattern with some of the colonised follicles displaying partial CD10 positivity consistent with the presence of residual GC B-cells.

With the exception of one case (grade 3B), all other thyroid FL were grade 3A (Figure 2C), and all showed predominantly a nodular growth pattern, and also prominent lymphoepithelial lesions including "MALT balls" (Figure 2). Like classic FL, *BCL2*-tr+v*e* thyroid FL expressed both CD10 and BCL6, albeit a single case with both *BCL2* and *BCL6* translocations was CD10 negative (Figure 2). Of the 15 *BCL2*-tr-ve FL, only 6 showed CD10 expression, with the remaining cases negative for CD10 including 7 and 2 with and without *BCL6* translocation respectively (Figure 2B,C). The FL diagnosis in these cases including those negative for both *BCL2* and *BCL6* translocations was supported by observation of expression of other GC markers (BCL6, HGAL, LMO2, GCET1, STMN1) in neoplastic B-cells within and outside B-cell follicles (Figure 2B, Figure S2). In contrast, none of these GC markers was positive in the neoplastic B-cells outside B-cell follicles in 21 cases of thyroid EMZL examined.

Thyroid DLBCL were unremarkable, all negative for *BCL2* translocation and 4 with *BCL6* translocation. Of the 34 cases investigated, 27 and 17 showed BCL6 and CD10 expression by immunohistochemistry respectively.

**Mutation signature among different thyroid B-cell lymphomas**

All somatic variants including synonymous, non-synonymous, indels and UTR changes were included in the mutation load analysis (Table S5). Overall, the mutation load was significantly higher in DLBCL than FL ($P$=0.006) and EMZL ($P$=0.005), but no significant difference between the two latter groups (Figure 3A). As many of the genes (n=37) investigated are targets of the somatic hypermutation (SHM) process, a separate analysis of mutations in these genes was performed, and this showed a

similar trend with DLBCL cases having a significantly higher mutation load in SHM targets than FL (*P*=0.021) and EMZL (*P*=0.014) (Figure S3).

We next compared the mutation signature among the three lymphoma groups by combining all the somatic single base substitutions of each group together as none of the individual cases had sufficient number of variants for such analysis. As expected, the cytidine deaminase (AID) associated mutation signature SBS84 was similarly found among the three lymphoma groups (Figure S3)[21]. Similarly, the clock-like/age related mutation signature SBS5 was also high among the three lymphoma groups [21].

**Mutation profile among different thyroid B-cell lymphomas**

The pathogenic mutations were compared among the three lymphoma groups with subset analysis according to translocation status.

Remarkably, there was a considerable overlap in the overall mutation profile among thyroid EMZL, *BCL2*-tr-ve FL and DLBCL, with frequent mutations in *TET2, IGLL5, TNFRSF14, CD274, GNA13, KLF2, TNFAIP3* and *FAS* (Figure 3A, Figure 4A, Figures S4&S5). Such overlap in mutation profile among the three groups was also seen in the genes not targeted by the SHM process (Figure 4A, Figure S4). Apart from a few genes, there was no significant difference in the mutation frequencies of the vast majority of genes between EMZL and *BCL2*-tr-ve FL, nor between *BCL2*-tr-ve FL and DLBCL (Figure 3B, Figure 4A). Similarly, there was no significant difference in the mutation profile between *BCL2*-tr-ve FL with and without *BCL6* translocation, nor between EMZL with and without *BCL6* translocation (Figure 3B, Figure S6). Nonetheless, thyroid DLBCL showed a significantly higher incidence of mutation in several genes (*SGK1*, *KLHL6*, *B2M*, *EBF1*, *SOCS1*, *FOXO1*, *P2RY8*, *DUSP2*, *KRAS*, *CD58*) than thyroid EMZL (Figure 3B, Figure 4A).

In contrast, *BCL2*-tr+ve FL of the thyroid showed frequent *BCL2*, *KMT2D*, *CREBBP*, *EZH2*, *TNFRSF14*, but not *TET2, CD274* and *IGLL5* mutations (Figure 3B, Figure 4A), similar to the mutation profile of nodal FL [22]. Nonetheless, all these thyroid cases were associated with HT as evidenced by clinical, laboratory and histological investigations, with 4/5 cases at early stage (IE=2, IIE=2), supporting their thyroid origin (Table S4).

Analysis of co-occurrence of the mutations revealed a number of significant associations and mutual exclusions (Figure 4B). For example, *TET2* mutation was significantly associated with *CD274*, *TNFAIP3*, *TNFRSF14* and *IGLL5* changes, and *CD274* mutation was further significantly associated with *TNFRSF14*, *PABPC1*, *TNFAIP3*, *FAS* and *KLF2* changes, but mutually exclusive from *KLHL6* and *B2M* changes (Figure 4B).

**Distinct genomic configuration of *BCL6* translocation between thyroid FL and EMZL**

The genomic configuration of *BCL6* translocation in 8 FL and 10 EMZL were investigated by TLC-NGS, and a further 2 FL were studied by a customised NGS panel (Figure 5, Figure 6).

Among the 10 FL with *BCL6* translocation, 3 showed genomic fusion between the *BCL6* intron 1 and the centromeric *IGHA1* region including 3'regulatory region 1 (3'RR1) super-enhancer in the same orientation, and this genomic configuration may cause *BCL6* transactivation due to super-enhancer hijack [23] (Figure 5). A further 5 cases displayed genomic fusion between *BCL6* intron 1 or its upstream 5′UTR region and either the 5′ regions of partner genes (*HSP90AA1, HMGA1, ZBTB38*) or the 3′UTR of *MIR29A* in the same orientation, and these genomic configurations represented a promoter substitution thus placing *BCL6* under the transcriptional control of its translocation partner. In the remaining 2 cases, 1 case showed fusion between the *BCL6* intron 1 and the

centromeric *IGHJ6* region in the same orientation, and the juxtaposed *IGHJ* region did not contain the Eμ super enhancer, thus lacking apparent mechanism to transactivate *BCL6* expression. In the other remaining case, the translocation placed an upstream region of the *BCL6* gene between the *IGH* and *IGK,* and the translocation did not involve any *BCL6* coding exons thus unlikely affecting BCL6 expression (Figure 5).

Among the 10 *BCL6*-tr+ve EMZLs, 5 cases showed genomic fusion between *BCL6* intron-1 or its upstream 5′UTR region, and the centromeric region of *IGHJ6* or D2-8 in the same orientation (Figure 6). As the translocated *IGHJ* and D2-8 region did not contain the Eμ super enhancer, these translocations lacked any apparent mechanism to drive constitutive *BCL6* expression. A further 2 cases displayed genomic fusion between the upstream of the *BCL6* 5′UTR region and its partner gene (upstream of *GRHPR* or upstream of *IGLL5*) in an opposite orientation, with no obvious evidence of super-enhancer hijack that may drive constitutive *BCL6* transactivation (Figure 6). In the remaining 3 cases, the translocation fused the *BCL6* 5'UTR or intron 1 to different partner genes in the same orientation (intron 2 of *SGK1* and *GAPDH* and intron 1 of *SMC4*), with the latter one potentially representing a promoter substitution.

In addition, TLC-NGS also identified additional chromosome translocations in 4 cases of the above *BCL6*-tr+ve thyroid lymphomas including 3 FL and 1 EMZL (Figure S7). One of these FL showed *IGH*::*BCL2* and the other two revealed an *IGH* involved translocation – one in association with *BTG2* but not involving its coding exons, and the remaining one in association with *IGK*. The EMZL case showed *IGH*::*SOX5,* with genomic configuration potentially driving *SOX5* expression (Figure S7).

**Potential impact of genetic changes on FL phenotype**

As many of the genes frequently altered in primary thyroid lymphoma are critical for the GC B-cell development, these genetic changes may potentially affect the maturation process of GC B cells, hence determining their differentiation stages that undergo malignant transformation. To investigate this, we first examined the expression pattern of *TET2*, *CD274*, *TNFRSF14*, *BCL6* and *MME* (CD10) in various normal GC B-cell subsets using the single cell transcriptomic data from human tonsils [24]. Interestingly, these genes showed a similar trend of expression across different GC B-cell subsets, being abundantly expressed in proliferating dark zone (DZ) GC B cells, reaching the highest expression level in DZ non-proliferating GC B cells and DZ to LZ (light zone) transition cells, then declined to the lowest level in LZ proliferating and LZ-to-DZ transition GC B-cell subsets (Figure 7).

The expression of the above genes must be tightly regulated, and their coordinated alterations are deemed critical in GC B-cell maturation and peripheral tolerance. As *TET2* mutation in primary thyroid lymphoma is an early event [3,5], its inactivation by mutations may cause genome-wide hypermethylation, thus potentially affect the above gene expression. To explore this, we examined above gene expression in *Tet2* deficient mouse GC B cells from a previous study [17]. In comparison with the wildtype mouse GC B cells, the *Tet2* deficient mouse GC B cells showed a higher level of methylation in *Irf4* (promoter), *Cd274* (gene body, introns) and *Mme* (CD10) (CpG site) and a reduced expression of these genes (Figure 8). However, there was no significant alteration in the methylation profile and expression of *Tnfrsf14* in the *Tet2* deficient mouse GC B cells.

**Correlation analysis of clinical, pathological and genetic data.**

A history of HT was present at a similar rate among thyroid EMZL (38/40=95%), FL (17/21=81% ) and DLBCL (28/34=82%) (Table S4). The average duration of HT was significantly higher in *BCL6*-tr-ve EMZL than the *BCL6*-tr+ve EMZL ($P$=0.008). Apart from that the DLBCL group showed a significant higher level of serum LDH than EMZL ($P$=0.005), and elevated sIL-2R than both FL ($P$=0.005) and

EMZL (*P*= 0.0000022), there were no significant differences among the standard clinical and laboratory parameters including TgAb and TPOAb among the three lymphoma groups

**DISCUSSION**

By investigating the genetic changes of primary thyroid EMZL, FL and DLBCL, we have unravelled several novel observations: 1) apart from *BCL2*-tr+ve FL, there is a remarkable overlap in the mutation profile among *BCL2*-tr-ve FL, EMZL, and DLBCL of the thyroid; 2) the core of these commonly mutation genes involves *TET2*, *TNFRSF14* and *CD274,* distinguishing them from other B-cell lymphomas including those at other mucosal sites; 3) *BCL6* translocation is recurrently seen in both thyroid FL and EMZL, but there is a fundamental difference in its genomic configuration between the two lymphoma entities. As many of these frequent genetic changes target genes that regulate B-cell maturation and tolerance in the peripheral lymphoid tissues, the above novel findings offer significant molecular insights into the pathogenesis of these thyroid lymphomas.

Like nodal FL, the thyroid *BCL2*-tr+ve FLs showed frequent mutations in *BCL2*, *TNFRSF14*, *KMT2D*, *CREBBP* and *EZH2*. Intriguingly, none of these thyroid *BCL2*-tr+ve FLs showed *TET2* and *CD274* mutations. It is important to note that these *BCL2*-tr+ve FLs were associated with HT and mainly at early clinical stages, not secondary to a systemic nodal disease. As *BCL2* translocation is an early event in FL development, occurring at the pre-B cell stage due to erroneous *IGH* VDJ recombination, it is pertinent to speculate that the aberrant *BCL2* over-expression caused by the translocation may favour the subsequent genetic changes with cooperative oncogenic activities, thus giving rise to a unique mutation pattern seen in all *IGH*::*BCL2* positive neoplasms including *in situ* follicular B-cell neoplasm, FL and transformed FL [12,25–29].

The remarkable overlap in the mutation profile (*TET2*, *IGLL5, TNFRSF14, CD274, GNA13, KLF2, TNFAIP3, FAS*) (Figure 3A) among *BCL2*-tr-ve FL, EMZL and DLBCL of the thyroid is intriguing, but biologically plausible. As these lymphomas originate from a common background of HT, their development most likely involves the same pathological process of autoimmunity that underpins HT. HT is characterised by development of autoreactive B-cells, and histologically extensive GC reactions, a process critically depending on T-helper cells. The molecular mechanisms that underpin the breach of peripheral tolerance may drive the evolution of autoreactive B cells and their clonal expansion. As B cells undergo reiterative GC reactions and relentless exposure to SHM activities, this may lead to acquisition of genetic abnormalities, eventual malignant transformation. In this context, the occurrence of malignant B-cell clone can be viewed as a part of the overall autoimmune process, but an extreme presentation. Thus, the overlapping mutation profile among *BCL2*-tr-ve FL, EMZL and DLBCL of the thyroid is likely driven by their common aetiology, i.e. the pivotal pathological process associated with HT.

In support of the above speculation, several genes among those frequently mutated in thyroid lymphoma are involved in the governance of peripheral tolerance. *CD274* (PD-L1) and *TNFRSF14* encode ligands for co-inhibitory surface receptor PD1 and BTLA on T-helper cells, respectively, and their inactivation by somatic mutation/deletion most likely constrain their negative regulation on T-helper cell function. PD-L1 deficiency or impairing PD1/PD-L1 interaction can cause autoimmune disorders in animal models [30,31]. Similarly, immune checkpoint inhibitors, particularly anti-PD1 antibody, frequently cause cancer patients to develop autoimmune thyroiditis and/or autoantibodies including anti-thyroperoxidase and anti-thyroglobulin [32,33]. Moreover, patients with germline *PD1* or *CD274* (PD-L1) loss-of-function mutations show early-onset endocrine autoimmunity [34,35]. *Cd274* deficiency in B cells appears to promote T-helper cell function, consequently enabling B cells a growth advantage [36,37]. Similarly, *Tnfrsf14* deficient B cells gain an enhanced growth advantage due to exaggerated T-cell help through increased CD40/CD40L co-

stimulation [38,39]. The concurrent inactivation of both *CD274* (PD-L1) and *TNFRSF14* in thyroid lymphomas may synergise in their enhancement of T-helper cell function, thus breaching peripheral tolerance and providing growth advantage to autoreactive B cells.

The above lymphomagenic process is likely augmented by the concurrent loss-of-function mutations in *TNFAIP3, KLF2* and *FAS. TNFAIP3* encodes a global negative regulator of the canonical NF-κB activation pathway and attenuates signalling transduction from several surface receptors including BCR, TNFR, TLR and IL1βR by inactivating their downstream signalling molecules through its ubiquitin editing activities [40]. Similarly, *KLF2* encodes a transcription factor/repressor that can negatively regulate NF-κB and NOTCH2 activities triggered by a range of surface receptor signalling [41]. *FAS* encodes a surface receptor for apoptosis signalling and mutant *FAS* can act as a dominant-negative, preventing FAS interaction with its downstream adaptor molecule FADD to mediate apoptosis [42]. Taken together, TNFAIP3, KLF2 and FAS inactivation may promote the apoptosis evasion of autoreactive B-cells and their clonal expansion [43].

The above mutations may also bear major impact on the histological presentation of lymphoma. Deficiency of *Tnfrsf14* or *Cd274* alone increases GC B-cell competitiveness in mice [36,38]. A combined inactivation of both *CD274* (PD-L1) and *TNFRSF14* in B cells may significantly enhance their entry, expansion and retention in B-cell follicles due to enhanced T-helper cell signals [31]. These biological impacts may underpin the follicular growth pattern of thyroid FL as well as the extensive follicular colonisation of thyroid EMZL. In this context, it is pertinent to point out that follicular colonisation in thyroid EMZL is the most prominent among EMZL of various sites, often involving most or majority of B-cell follicles, thus posing significant difficulty in differential diagnosis from *BCL2*-tr-ve FL [2].

In a similar context, paediatric-type follicular lymphoma (PTFL) and paediatric nodal marginal zone lymphoma (PNMZL) also exhibit substantial overlap in their clinical, morphological and genetic features [44,45] . The shared genetic changes between the two lymphomas have been used to argue for considering these different lymphomas as a single biological entity with variations in their histological presentations[44,45]. The somatic genetic alterations and tumor microenvironmental factors that influence GC entry (for example T-cell dependent B-cell activation) and GC exit (via BCL6 downregulation) are likely to have a major impact on the phenotypic presentation of these lymphomas. However, existing studies have largely focused on mutations within coding gene sequences, while other potentially relevant genetic changes, such as somatic mutations in *BCL6* transcriptional regulatory (non-coding) regions that could affect GC exit [46,47], remain to be explored . Thus, the currently available data are not sufficient to support considering these lymphomas as a single biological entity.

The finding of recurrent *BCL6* translocation in EMZL is rather paradoxical as BCL6 is a master transcriptional factor that orchestrates the GC reaction while repressing the plasma cell differentiation programme [9,10], hence maintaining the GC phenotype. Our finding of significant differences in the genomic configuration of *BCL6* translocation between thyroid FL and EMZL provides a plausible explanation. In thyroid FL, majority of *BCL6* translocations place the *BCL6* coding exons under the transcriptional control of the IGH switch region super enhancer (3'RR1) or its partner genes, known as super enhancer hijack and promoter substitution respectively. Among the five cases with *BCL6* translocation genomic configuration showing promoter substitution, all the partner genes (*HSP90AA1*, *HMGA1*, *ZBTB38*, *MIR29A*) appear to be highly expressed in B cells [48–53]. These genomic configurations most likely enable BCL6 constitutive expression. In contrast, majority of *BCL6* translocations in thyroid EMZL juxtapose the *BCL6* gene to the IGHJ/IGHD region without encompassing the Eμ enhancer or partner genes in an opposite orientation. In the three cases of

thyroid EMZL where *BCL6* is placed in the same orientation with its partner gene, two cases involved coding exons of the partner gene (*GAPDH*, *SGK1*), potentially resulting in chimeric transcripts and possible protein products with unknown function. While the remaining case with the partner gene *SMC4* may represent a true promoter substitution, but SMC4 appears not to be highly expressed in B-cells [49,50]. Overall, *BCL6* translocation in thyroid EMZL lacks the apparent genomic configuration that enables *BCL6* constitutive expression, hence minimal impact on the lymphoma phenotypic presentation.

*TET2*, *CD274* and *TNFRSF14* inactivation may also affect the GC B-cell maturation process, potentially influencing their differentiation stage that undergo malignant transformation, and hence the neoplastic cell immunophenotype. During normal GC reaction as shown in tonsils, the down regulation of *CD274* and *TNFRSF14* expression in LZ centrocytes may dampen their inhibitory effect on T-follicular helper cells, allowing them to receive more T-cell help, preparing for GC exit or re-entry to DZ for further SHM. *Tet2* deficiency increased the proportion of GC centrocytes and impaired GC exit [54]. Although the molecular mechanism how *Tet2* deficiency dysregulates the GC reaction is not fully understood, *Tet2* deficient mouse GC B cells showed an increased level of DNA methylation in *Cd274, Mme* (CD10) and *Irf4*, accompanied by their reduced expression in comparison with wild type controls [17]. This, together with the inactivation of both *CD274* and *TNFRSF14,* may promote GC B-cell maturation process toward LZ centrocytes and memory B-cell differentiation. On the other hand, *BCL6* constitutive expression by translocation and/or other mechanisms may prevent the late GC B-cells from GC exit by repressing transcription factors (BLIMP1) critical for plasma cell differentiation [9,10]. Taken together, it is conceivable that these genetic changes may cooperate in their oncogenic activities, promoting the GC B-cell differentiation process, but impairing their GC exit, thus favouring malignant transformation of the late GC B-cell subsets. This may potentially explain why a high proportion of *BCL2*-tr-ve FL of the thyroid is CD10 negative.

In conclusion, our findings offer significant molecular insights into the pathogenesis of thyroid lymphomas, bridging autoimmunity, somatic genetic changes and lymphomagenesis together, and potentially explaining the overlap of histological presentations between thyroid EMZL and FL.

**REFERENCES**


1. Watanabe N, Noh JY, Narimatsu H, et al. Clinicopathological features of 171 cases of primary thyroid lymphoma: a long-term study involving 24 553 patients with Hashimoto's disease. Br J Haematol. 2011;153(2):236-243.
2. Bacon CM, Diss TC, Ye H, et al. Follicular Lymphoma of the Thyroid Gland. Am J Surg Pathol. 2009;33(1):22-34.
3. Wu F, Watanabe N, Tzioni MM, et al. Thyroid MALT lymphoma: self-harm to gain potential T-cell help. Leukemia. 2021;35(12):3497-3508.
4. Moody S, Thompson JS, Chuang SS, et al. Novel GPR34 and CCR6 mutation and distinct genetic profiles in MALT lymphomas of different sites. Haematologica. 2018;103(8):1329-1336.
5. Tzioni MM, Watanabe N, Chen Z, et al. Primary thyroid B-cell lymphoma: molecular insights into its clonal evolution and relapse. J Pathol. 2025;265(2):123-131.
6. Ye H, Remstein ED, Bacon CM, Nicholson AG, Dogan A, Du MQ. Chromosomal translocations involving BCL6 in MALT lymphoma. Haematologica. 2008;93(1):145-146.
7. Dierlamm J, Pittaluga S, Stul M, et al. BCL6 gene rearrangements also occur in marginal zone B-cell lymphoma. Br J Haematol. 1997;98(3):719-725.
8. Suzuki A, Hirokawa M, Higashiyama T, et al. Flow cytometric, gene rearrangement, and karyotypic analyses of 110 cases of primary thyroid lymphoma: a single-institutional experience in Japan. Endocr J. 2019;66(12):1083-1091.
9. Parekh S, Polo JM, Shaknovich R, et al. BCL6 programs lymphoma cells for survival and differentiation through distinct biochemical mechanisms. Blood. 2007;110(6):2067-2074.
10. Shapiro-Shelef M, Lin KI, Mcheyzer-Williams LJ, Liao J, Mcheyzer-Williams MG, Calame K. Blimp-1 Is Required for the Formation of Immunoglobulin Secreting Plasma Cells and Pre-Plasma Memory B Cells. Immunity. 2003;19(4):607-620.

11. Cucco F, Clipson A, Kennedy H, et al. Mutation screening using formalin-fixed paraffin-embedded tissues: a stratified approach according to DNA quality. Lab Invest. 2018;98(8):1084-1092.

12. Cucco F, Barrans S, Sha C, et al. Distinct genetic changes reveal evolutionary history and heterogeneous molecular grade of DLBCL with MYC/BCL2 double-hit. Leukemia. 2019;34(5):1329-1341.

13. Zhang C, Stelloo E, Barrans S, et al. Non-IG::MYC in diffuse large B-cell lymphoma confers variable genomic configurations and MYC transactivation potential. Leukemia. 2024;38(3):621-629.

14. Díaz-Gay M, Vangara R, Barnes M, et al. Assigning mutational signatures to individual samples and individual somatic mutations with SigProfilerAssignment. Bioinformatics. 2023;39(12):btad756.

15. Allahyar A, Pieterse M, Swennenhuis J, et al. Robust detection of translocations in lymphoma FFPE samples using targeted locus capture-based sequencing. Nat Commun. 2021;12(1):3361.

16. Mikulasova A, Kent D, Trevisan-Herraz M, et al. Epigenomic translocation of H3K4me3 broad domains over oncogenes following hijacking of super-enhancers. Genome Res. 2022;32(7):1343-1354.

17. Fujisawa M, Nguyen TB, Abe Y, et al. Clonal germinal center B cells function as a niche for T-cell lymphoma. Blood. 2022;140(18):1937-1950.

18. Love MI, Huber W, Anders S. Moderated estimation of fold change and dispersion for RNA-seq data with DESeq2. Genome Biol. 2014;15(12):550.

19. Mayakonda A, Lin DC, Assenov Y, Plass C, Koeffler HP. Maftools: efficient and comprehensive analysis of somatic variants in cancer. Genome Res. 2018;28(11):1747-1756.

20. Isaacson PG, Androulakis-Papachristou A, Diss TC, Pan L, Wright DH. Follicular colonization in thyroid lymphoma. Am J Pathol. 1992;141(1):43-52.

21. Alexandrov LB, Kim J, Haradhvala NJ, et al. The repertoire of mutational signatures in human cancer. Nature. 2020;578(7793):94-101.

22. Perrett M, Edmondson C, Okosun J. Biology of follicular lymphoma: insights and windows of clinical opportunity. Hematology Am Soc Hematol Educ Program. 2022;2022(1):688-694.

23. Kasprzyk ME, Sura W, Dzikiewicz-Krawczyk A. Enhancing B-Cell Malignancies-On Repurposing Enhancer Activity towards Cancer. Cancers (Basel). 2021;13(13):3270.

24. Massoni-Badosa R, Aguilar-Fernández S, Nieto JC, et al. An atlas of cells in the human tonsil. Immunity. 2024;57(2):379-399.e18.

25. Okosun J, Bödör C, Wang J, et al. Integrated genomic analysis identifies recurrent mutations and evolution patterns driving the initiation and progression of follicular lymphoma. Nat Genet. 2014;46(2):176-181.

26. Pasqualucci L, Khiabanian H, Fangazio M, et al. Genetics of Follicular Lymphoma Transformation. Cell Rep. 2014;6(1):130-140.

27. Bouska A, Zhang W, Gong Q, et al. Combined copy number and mutation analysis identifies oncogenic pathways associated with transformation of follicular lymphoma. Leukemia. 2017;31(1):83-91.

28. Kridel R, Chan FC, Mottok A, et al. Histological Transformation and Progression in Follicular Lymphoma: A Clonal Evolution Study. PLoS Med. 2016;13(12):e1002197.

29. Dobson R, Wotherspoon A, Liu SA, et al. Widespread in situ follicular neoplasia in patients who subsequently developed follicular lymphoma. J Pathol. 2022;256(4):369-377.

30. Sage PT, Schildberg FA, Sobel RA, Kuchroo VK, Freeman GJ, Sharpe AH. Dendritic Cell PD-L1 Limits Autoimmunity and Follicular T Cell Differentiation and Function. J Immunol. 2018;200(8):2592-2602.

31. Martinov T, Swanson LA, Breed ER, et al. Programmed Death-1 Restrains the Germinal Center in Type 1 Diabetes. J Immunol. 2019;203(4):844-852.

32. Chalan P, Di Dalmazi G, Pani F, De Remigis A, Corsello A, Caturegli P. Thyroid dysfunctions secondary to cancer immunotherapy. J Endocrinol Invest. 2018;41(6):625-638.

33. De Moel EC, Rozeman EA, Kapiteijn EH, et al. Autoantibody development under treatment with immune-checkpoint inhibitors. Cancer Immunol Res. 2019;7(1):6-11.

34. Ogishi M, Kitaoka K, Good-Jacobson KL, et al. Impaired development of memory B cells and antibody responses in humans and mice deficient in PD-1 signaling. Immunity. 2024;57(1):2790-2807.e15.

35. Johnson MB, Ogishi M, Domingo-Vila C, et al. Human inherited PD-L1 deficiency is clinically and immunologically less severe than PD-1 deficiency. J Exp Med. 2024;221(6):e20231704.

36. Shi J, Hou S, Fang Q, Liu X, Liu X, Qi H. PD-1 Controls Follicular T Helper Cell Positioning and Function. Immunity. 2018;49(2):264-274.e4.

37. Wan Z, Lin Y, Zhao Y, Qi H. TFH cells in bystander and cognate interactions with B cells. Immunol Rev. 2019;288(1):28-36.

38. Mintz MA, Felce JH, Chou MY, et al. The HVEM-BTLA Axis Restrains T Cell Help to Germinal Center B Cells and Functions as a Cell-Extrinsic Suppressor in Lymphomagenesis. Immunity. 2019;51(2):310-323.e7.

39. Kennedy R, Klein U. A T Cell-B Cell Tumor-Suppressive Axis in the Germinal Center. Immunity. 2019;51(2):204-206.

40. Du MQ. MALT lymphoma: A paradigm of NF-κB dysregulation. Semin Cancer Biol. 2016;39:49-60.

41. Clipson A, Wang M, De Leval L, et al. KLF2 mutation is the most frequent somatic change in splenic marginal zone lymphoma and identifies a subset with distinct genotype. Leukemia. 2015;29(5):1177-1185.

42. Consonni F, Gambineri E, Favre C. ALPS, FAS, and beyond: from inborn errors of immunity to acquired immunodeficiencies. Ann Hematol. 2022;101(3):469-484.

43. Du MQ. EMZL at various sites: learning from each other. Blood. 2025;145(19):2117-2127.

44. Salmeron-Villalobos J, Egan C, Borgmann V, et al. A unifying hypothesis for PNMZL and PTFL: morphological variants with a common molecular profile. Blood Adv. 2022;6(16):4661-4674.

45. Lim S, Lim KY, Koh J, et al. Pediatric-Type Indolent B-Cell Lymphomas With Overlapping Clinical, Pathologic, and Genetic Features. Am J Surg Pathol. 2022;46(10):1397-1406.

46. Saito M, Gao J, Basso K, et al. A Signaling Pathway Mediating Downregulation of BCL6 in Germinal Center B Cells Is Blocked by BCL6 Gene Alterations in B Cell Lymphoma. Cancer Cell. 2007;12(3):280-292.

47. Bal E, Kumar R, Hadigol M, et al. Super-enhancer hypermutation alters oncogene expression in B cell lymphoma. Nature. 2022;607(7920):808-815.

48. Liston A, Papadopoulou AS, Danso-Abeam D, Dooley J. MicroRNA-29 in the adaptive immune system: Setting the threshold. Cell Mol Life Sci. 2012;69(21):3533-3541.

49. Schmiedel BJ, Singh D, Madrigal A, et al. Impact of Genetic Polymorphisms on Human Immune Cell Gene Expression. Cell. 2018;175(6):1701-1715.e16.

50. Monaco G, Lee B, Xu W, et al. RNA-Seq Signatures Normalized by mRNA Abundance Allow Absolute Deconvolution of Human Immune Cell Types. Cell Rep. 2019;26(6):1627-1640.e7.

51. Wong R, Bhattacharya D. ZBTB38 is dispensable for antibody responses. PLoS One. 2020;15(9):e0235183.

52. Tan LP, Wang M, Robertus JL, et al. miRNA profiling of B-cell subsets: specific miRNA profile for germinal center B cells with variation between centroblasts and centrocytes. Lab Invest. 2009;89(6):708-716.

53. De Martino M, Esposito F, Fusco A. Critical role of the high mobility group A proteins in hematological malignancies. Hematol Oncol. 2022;40(1):2-10.

54. Dominguez PM, Ghamlouch H, Rosikiewicz W, et al. TET2 Deficiency Causes Germinal Center Hyperplasia, Impairs Plasma Cell Differentiation, and Promotes B-cell Lymphomagenesis. Cancer Discov. 2018;8(12):1632-1653.

**FIGURE LEGENDS**

**Figure 1.** Histopathology of a representative primary thyroid extranodal marginal zone lymphoma of mucosa-associated lymphoid tissue (EMZL).

**A**: A thyroid EMZL without *BCL6* translocation (case EMZL-37) shows diffuse infiltration of neoplastic B-cells with prominent lymphoepithelial lesions including "MALT ball", and also extensive follicular colonisation. CD10 immunohistochemistry highlights residual germinal centre B cells, while neoplastic B-cells in the colonised follicle are CD10 negative. BCL6 positivity likely identifies both residual germinal centre B cells and the colonised neoplastic B cells.

**B**: A thyroid EMZL with *BCL6* translocation (case EMZL-04) displays diffuse infiltration of neoplastic B-cells with prominent lymphoepithelial lesions. CD21 immunohistochemistry highlights the colonized follicles that are virtually negative for CD10 but variable BCL6 expression, indicating total overrun by neoplastic B cells.

tr+ve: translocation positive, tr-ve: translocation negative; LEL: lymphoepithelial lesion.

**Figure 2**. Histopathology of representative primary thyroid follicular lymphoma (FL).

**A**: A *BCL2* translocation positive FL (case FL-05) shows follicular growth pattern and extensive lymphoepithelial lesions including "MALT ball" in the interfollicular region. The neoplastic cells including those involved in the lymphoepithelial lesions are strongly positive for CD10 and BCL2.

**B**: A *BCL2 and BCL6* translocation negative FL (case FL-19) displays vaguely follicular growth pattern with little involvement of the interfollicular region. The neoplastic B cells in both follicle centre and interfollicular regions are positive for CD10, BCL6 and HGAL.

**C**: Summary of immunophenotype of primary thyroid FL. CD10 is more often negative in *BCL2* translocation negative FL including those with *BCL6* translocation. *FL-04 showed no apparent neoplastic involvement in the interfollicular region.

tr+ve: translocation positive, tr-ve: translocation negative; LEL: lymphoepithelial lesion; FC: follicle centre; IF: interfollicular region; STMN1: Stathmin 1.

**Figure 3.** Comparison of mutation frequencies among different primary thyroid lymphomas.

**A**: Comparison of mutation frequencies among thyroid EMZL, FL and DLBCL. Only genes showing a frequency of potentially pathogenic mutation above 10% in any of these lymphoma groups are included, with the exception of *BCL2*, of which all variants are included.

**B**: Comparison of mutation frequency between subsets of thyroid EMZL, FL and DLBCL as indicated. In each comparison, all genes showing a mutation frequency above 10% in any of the two subsets included, with the exception of *BCL2*, of which all variants are included to highlight different mutation profiles among various comparisons. * denotes significant changes between subsets ($P \leq 0.05$).

FL: follicular lymphoma; DLBCL: diffuse large B-cell lymphoma; EMZL: extranodal marginal zone lymphoma of mucosa-associated lymphoid tissue; tr+ve: translocation positive, tr-ve: translocation negative.

**Figure 4.** Mutation profiles among different primary thyroid lymphoma.

**A**: Heatmap illustration of mutation profile among thyroid EMZL, FL and DLBCL. Please see Figure S4 for complete data illustration. Only genes showing a frequency of potentially pathogenic mutation above 10% in any of these lymphoma groups are included in the data presentation, with the exception of *BCL2*, of which all variants are included to allow informed comparison among subgroups. * and ** denote known and predicted somatic hypermutation targets respectively.

**B**: Correlation analysis of mutation seen in top 20 most frequently mutated genes in thyroid EMZL, FL and DLBCL. • denotes differences which were statistically significant ($P < 0.05$).

FL: follicular lymphoma; DLBCL: diffuse large B-cell lymphoma; EMZL: extranodal marginal zone lymphoma of mucosa-associated lymphoid tissue; tr+ve: translocation positive, tr-ve: translocation negative; SNV: single nucleotide variation; SHM: somatic hypermutation; N/A: not available.

**Figure 5.** Genomic configuration of *BCL6* translocation in primary thyroid FL. Genomic breakpoint sequencing analyses was performed by targeted locus capture-based next generation sequencing (TLC-NGS) or a customised NGS panel with sequence annotations based on human genome (hg19) together with IGH super enhancers according to Mikulasova et al [16]. FL: follicular lymphoma; cen: centromeric; tel: telomeric.

**Figure 6.** Genomic configuration of *BCL6* translocation in primary thyroid EMZL. Genomic breakpoint sequencing analyses was performed by targeted locus capture-based next generation sequencing (TLC-NGS) with sequence annotations based on human genome (hg19) together with IGH super enhancers according to Mikulasova et al [16]. EMZL: extranodal marginal zone lymphoma of mucosa-associated lymphoid tissue; cen: centromeric; tel: telomeric.

**Figure 7.** Re-analyses of single-cell RNA sequencing data of germinal centre (GC) B cells from the tonsil cell atlas project [24]. UMAP illustration shows the overall distribution of the indicated genes among various subsets of GC B cells. Violin plots with overlaid box plots compare the expression level of the indicated genes [*TET2*, *CD274*, *TNFRSF14*, *BCL6*, *MME* (CD10), and *CD40*] among various subsets of GC B-cells. DZ: dark zone; LZ: light zone; MBCs: memory B cells; PC: plasma cells; GCBC: germinal centre B cells.

**Figure 8.** Epigenomic and transcriptomic alterations in germinal centre B cells from Tet2-deficient and wild-type mice. GCB: germinal centre B cells.

**A.** Visualisations of base-resolution DNA methylation profiles at representative gene loci (*Mme*, *Cd274*, *Irf4*, and *Tnfrsf14*) derived from whole-genome bisulfite sequencing (WGBS) of GC B cells sorted from the spleens of *Tet2*-deficient ($Tet2^{-/-}$) and wild-type ($Tet2^{wt}$) mice. The y-axis represents base-resolution methylation levels derived from WGBS. Differentially methylated regions (q-value ≤ 0.25 and |methylation difference| > 30%) are highlighted with red squares.

**B.** Normalised expression values of the indicated genes based on DESeq2 analysis of RNA-seq data ($Tet2^{-/-}$, n=5; $Tet2^{wt}$, n=4)[17,18]. *, **, and n.s. indicate $p < 0.05$, $p < 0.01$, and not significant, respectively.

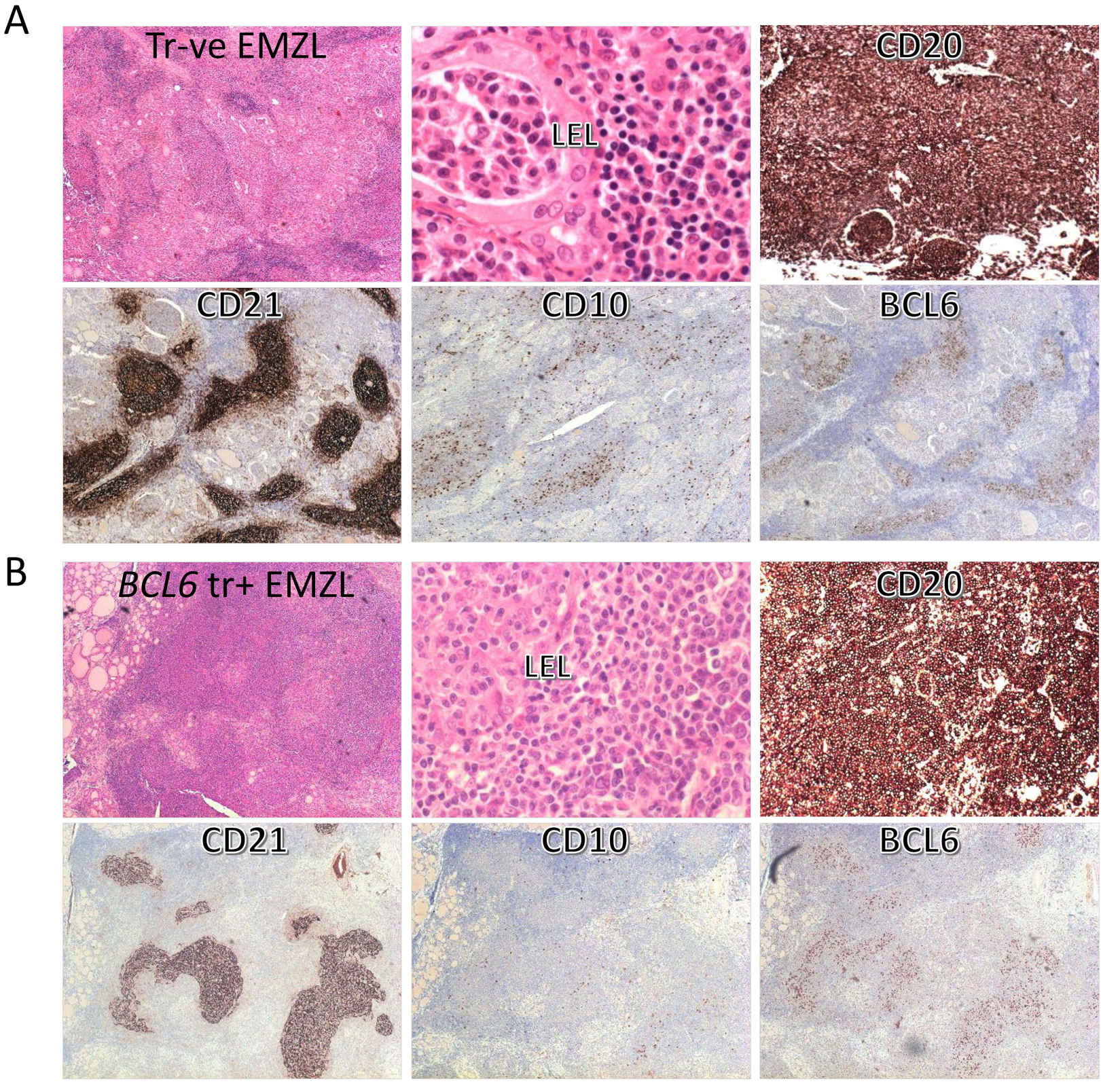
A
Tr-ve EMZL
LEL
CD20
CD21
CD10
BCL6
B
*BCL6* tr+ EMZL
LEL
CD20
CD21
CD10
BCL6

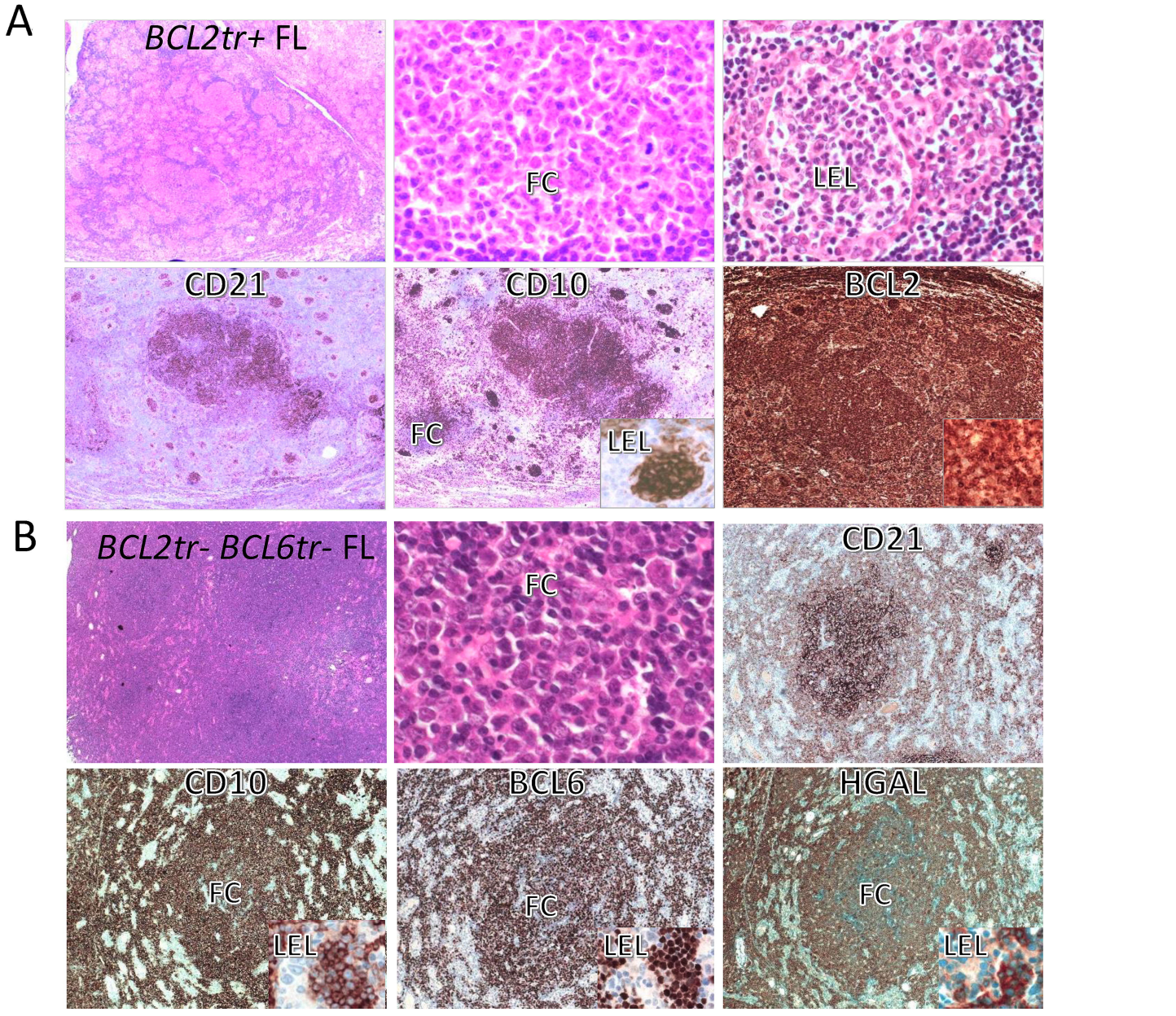
A
BCL2tr+ FL
FC
LEL
CD21
CD10
FC
LEL
BCL2
B
BCL2tr- BCL6tr- FL
FC
CD21
CD10
FC
LEL
BCL6
FC
LEL
HGAL
FC
LEL

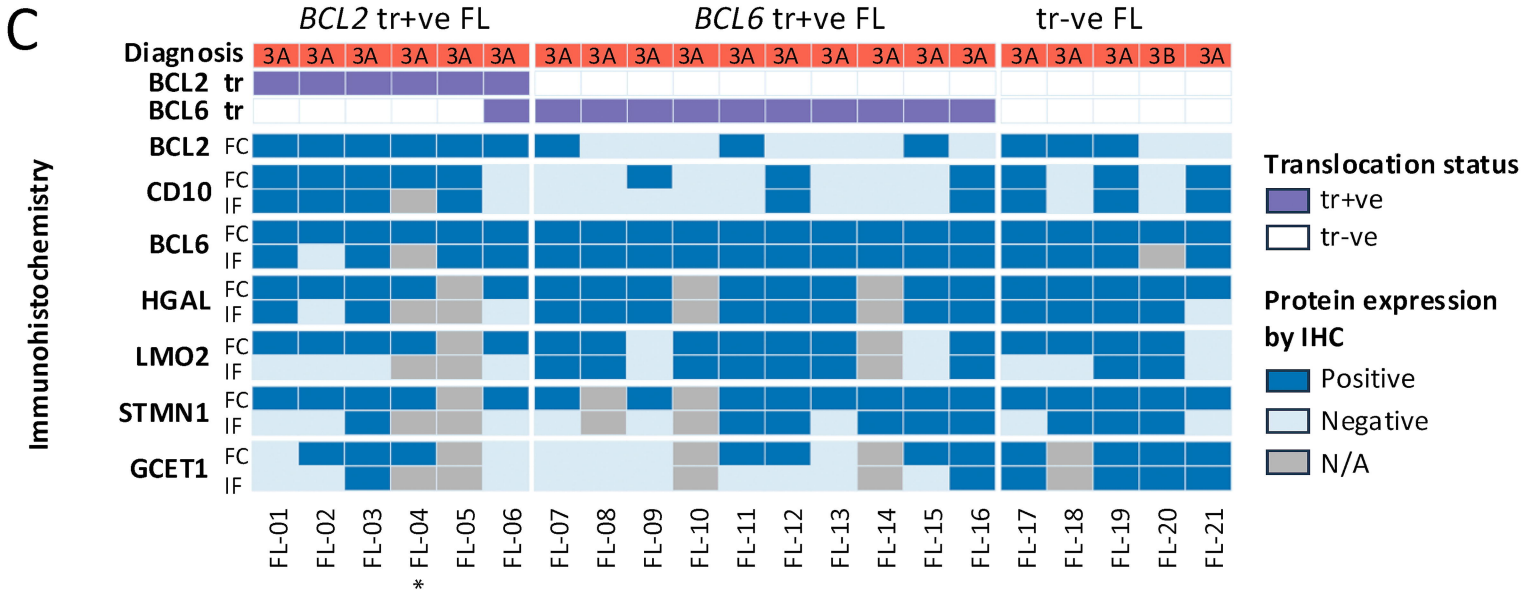
C
BCL2 tr+ve FL
BCL6 tr+ve FL
tr-ve FL
Diagnosis
3A 3A 3A 3A 3A 3A 3A 3A 3A 3A 3A 3A 3A 3A 3A 3A 3A 3A 3A 3B 3A
BCL2 tr
BCL6 tr
BCL2 FC
CD10 FC IF
BCL6 FC IF
HGAL FC IF
LMO2 FC IF
STMN1 FC IF
GCET1 FC IF
Immunohistochemistry
FL-01 FL-02 FL-03 FL-04 * FL-05 FL-06 FL-07 FL-08 FL-09 FL-10 FL-11 FL-12 FL-13 FL-14 FL-15 FL-16 FL-17 FL-18 FL-19 FL-20 FL-21
Translocation status
tr+ve
tr-ve
Protein expression by IHC
Positive
Negative
N/A

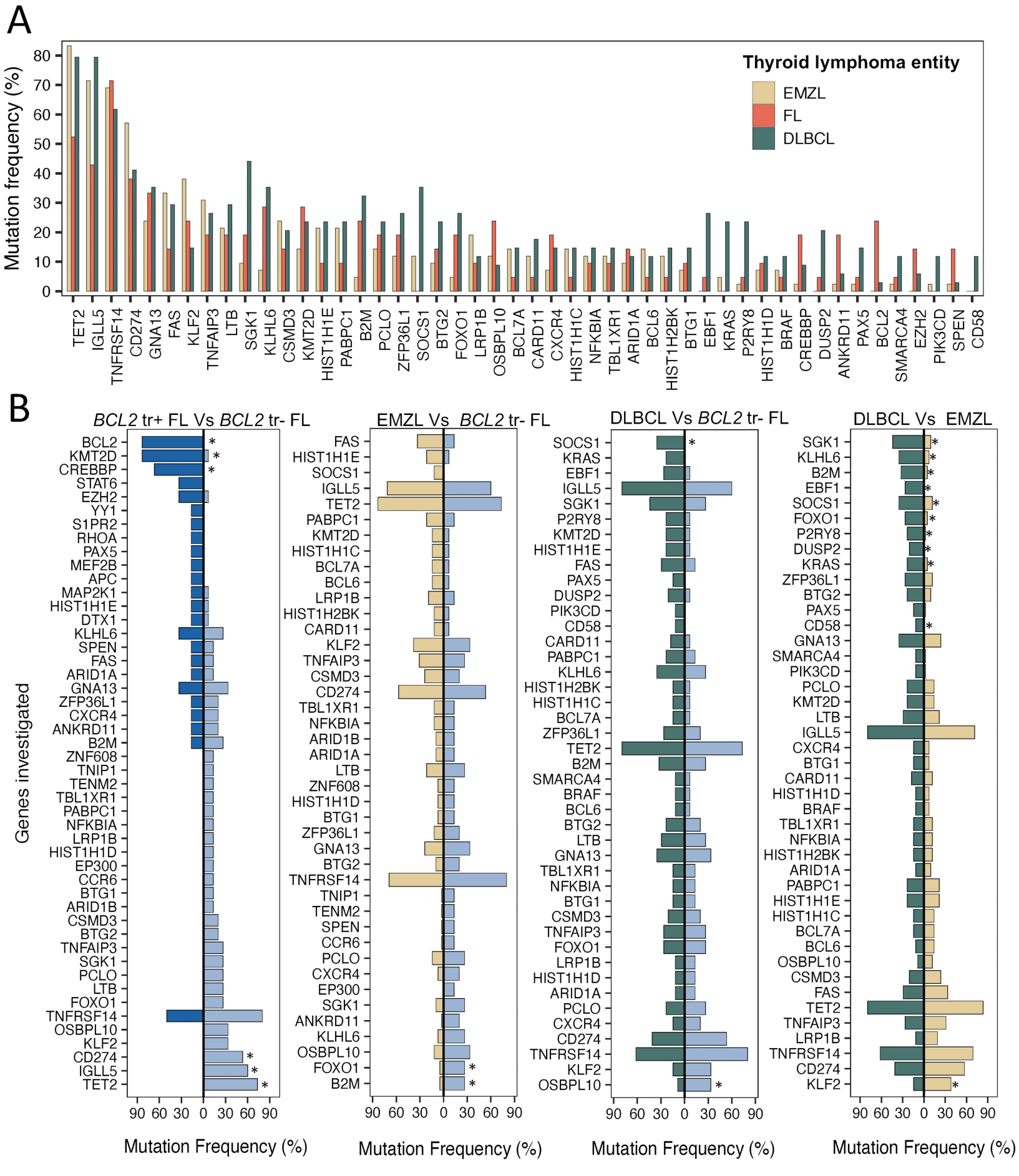
A
Mutation frequency (%)
Thyroid lymphoma entity
EMZL
FL
DLBCL
TET2 IGLL5 TNFRSF14 CD274 GNA13 FAS KLF2 TNFAIP3 LTB SGK1 KLHL6 CSMD3 KMT2D HIST1H1E PABPC1 B2M PCLO ZFP36L1 SOCS1 BTG2 FOXO1 LRP1B OSBPL10 BCL7A CARD11 CXCR4 HIST1H1C NFKBIA TBL1XR1 ARID1A BCL6 HIST1H2BK BTG1 EBF1 KRAS P2RY8 HIST1H1D BRAF CREBBP DUSP2 ANKRD11 PAX5 BCL2 SMARCA4 EZH2 PIK3CD SPEN CD58
B
BCL2 tr+ FL Vs BCL2 tr- FL
EMZL Vs BCL2 tr- FL
DLBCL Vs BCL2 tr- FL
DLBCL Vs EMZL
Genes investigated
Mutation Frequency (%)
Mutation Frequency (%)
Mutation Frequency (%)
Mutation Frequency (%)

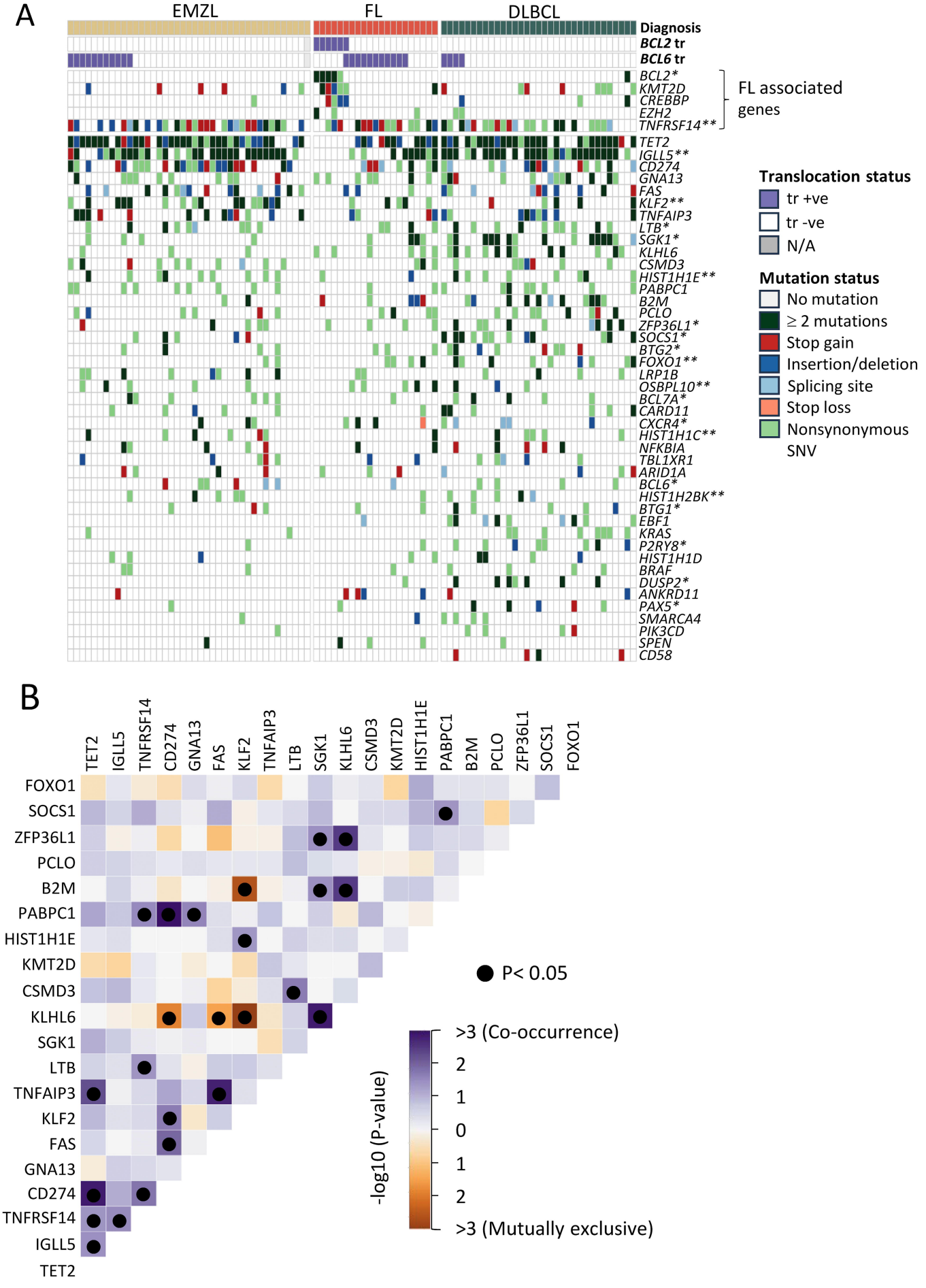
A
EMZL
FL
DLBCL
Diagnosis
BCL2 tr
BCL6 tr
BCL2*
KMT2D
CREBBP
EZH2
TNFRSF14**
FL associated genes
TET2
IGLL5**
CD274
GNA13
FAS
KLF2**
TNFAIP3
LTB*
SGK1*
KLHL6
CSMD3
HIST1H1E**
PABPC1
B2M
PCLO
ZFP36L1*
SOCS1*
BTG2*
FOXO1**
LRP1B
OSBPL10**
BCL7A*
CARD11
CXCR4*
HIST1H1C**
NFKBIA
TBL1XR1
ARID1A
BCL6*
HIST1H2BK**
BTG1*
EBF1
KRAS
P2RY8*
HIST1H1D
BRAF
DUSP2*
ANKRD11
PAX5*
SMARCA4
PIK3CD
SPEN
CD58
Translocation status
tr +ve
tr -ve
N/A
Mutation status
No mutation
≥ 2 mutations
Stop gain
Insertion/deletion
Splicing site
Stop loss
Nonsynonymous SNV
B
TET2
IGLL5
TNFRSF14
CD274
GNA13
FAS
KLF2
TNFAIP3
LTB
SGK1
KLHL6
CSMD3
KMT2D
HIST1H1E
PABPC1
B2M
PCLO
ZFP36L1
SOCS1
FOXO1
P< 0.05
-log10 (P-value)
>3 (Co-occurrence)
2
1
0
1
2
>3 (Mutually exclusive)

**FL-07**

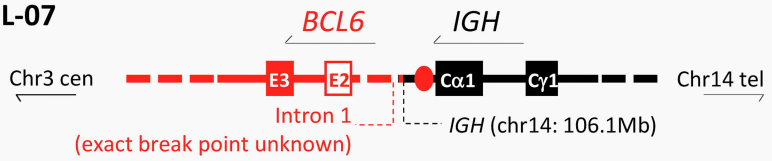


Enhance *BCL6* transcription due to the super enhancer at *IGHC*.

**FL-10**

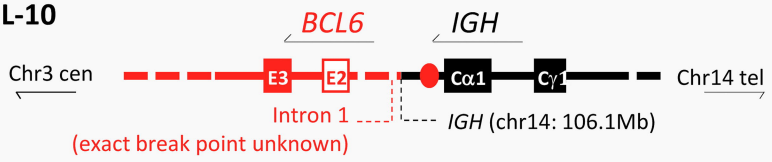


Enhance *BCL6* transcription due to the super enhancer at *IGHC*.

**FL-13**

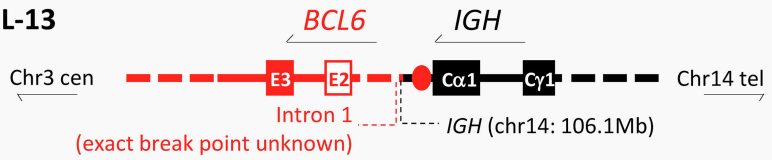


Enhance *BCL6* transcription due to the super enhancer at *IGHC*.

**FL-11**

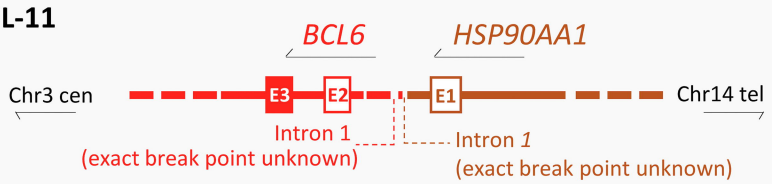


High HSP90AA1 expression in B cells, potentially enhance *BCL6* transcription due to promoter substitution

**FL-16**

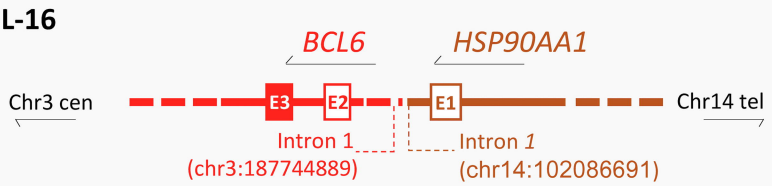


High HSP90AA1 expression in B cells, potentially enhance *BCL6* transcription due to promoter substitution

**FL-12**

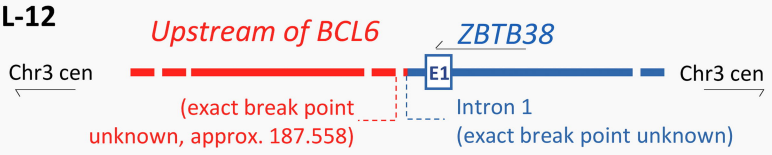


Moderate-high ZBTB38 expression in B-cells, potentially enhance *BCL6* transcription due to promoter substitution

**FL-09**

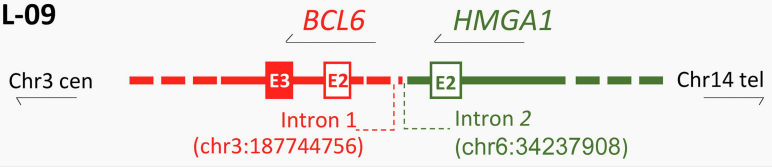


High HMGA1 expression in B cells, potentially enhance *BCL6* transcription due to promoter substitution

**FL-06**

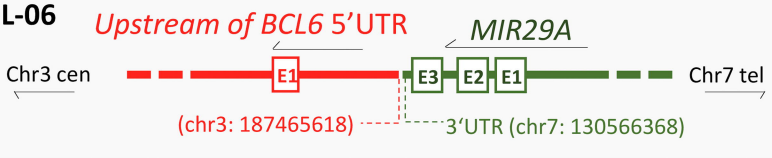


High MIR29A expression in B cells, and potentially enhance *BCL6* transcription due to promoter substitution

**FL-08**

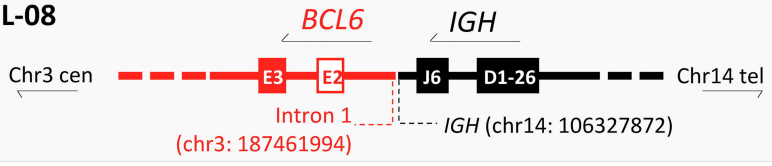


Breakpoint is telemeric of the Eμ, thus lack of *IG* super enhancer on derivative Chr3 to drive BCL6 constitutive expression

**FL-14**

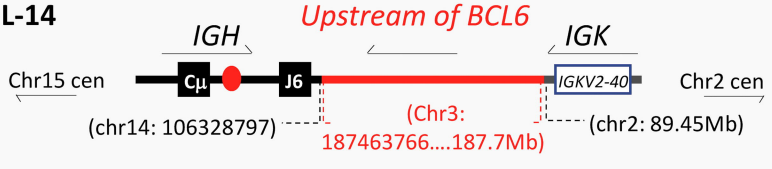


Not containing *BCL6* coding sequence, thus no impact on *BCL6* expression

**EMZL-03**

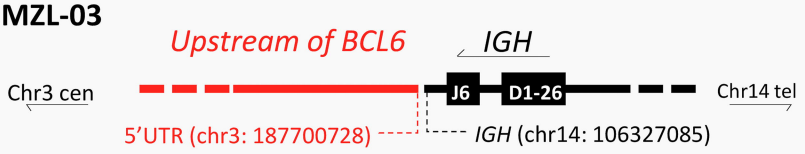


Breakpoint is telemeric of the Eμ, thus lack of *IG* super enhancer on derivative Chr3 to drive BCL6 constitutive expression

**EMZL-07**

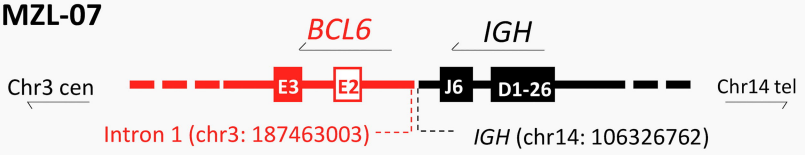


Breakpoint is telemeric of the Eμ, thus lack of *IG* super enhancer on derivative Chr3 to drive BCL6 constitutive expression

**EMZL-09**

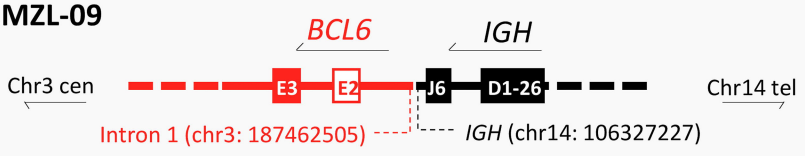


Breakpoint is telemeric of the Eμ, thus lack of *IG* super enhancer on derivative Chr3 to drive BCL6 constitutive expression

**EMZL-02**

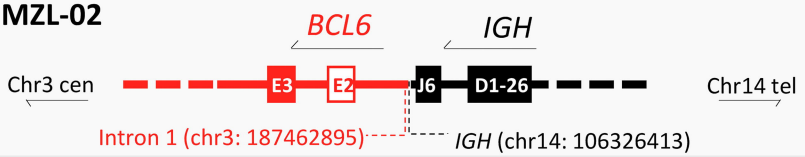


Breakpoint is telemeric of the Eμ, thus lack of *IG* super enhancer on derivative Chr3 to drive BCL6 constitutive expression

**EMZL-04**

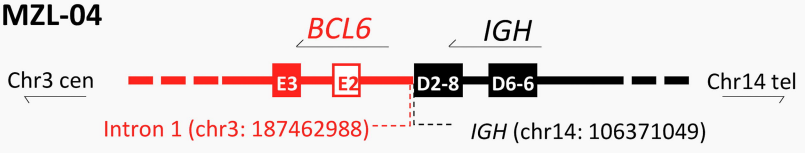


Breakpoint is telemeric of the Eμ, thus lack of *IG* super enhancer on derivative Chr3 to drive BCL6 constitutive expression

**EMZL-08**

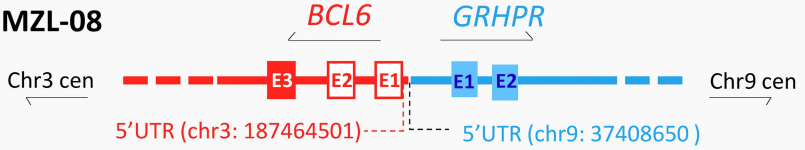


Opposite orientation, unlikely to enhance *BCL6* expression

**EMZL-05**


Does not contain *IGL* enhancer, unlikely to cause *BCL6* constitutive expression

**EMZL-06**

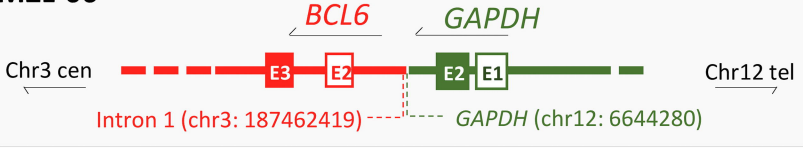


High GAPDH expression in B cells. Potentially producing chimeric transcripts and protein products with unknown function

**EMZL-10**

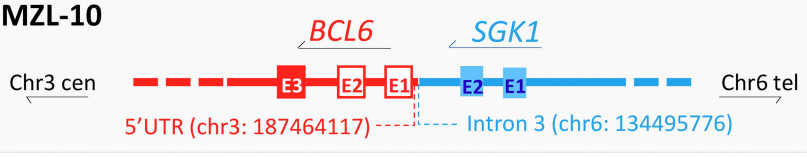


Very low SGK1 expression in B-cells. Potentially producing chimeric transcripts and protein products with unknown function

**EMZL-11**

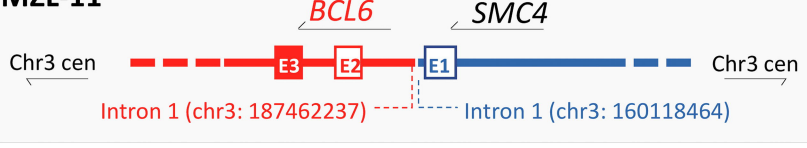


Low-moderate SMC4 expression in B-cells. Might enhance BCL6 expression due to promoter substitution?

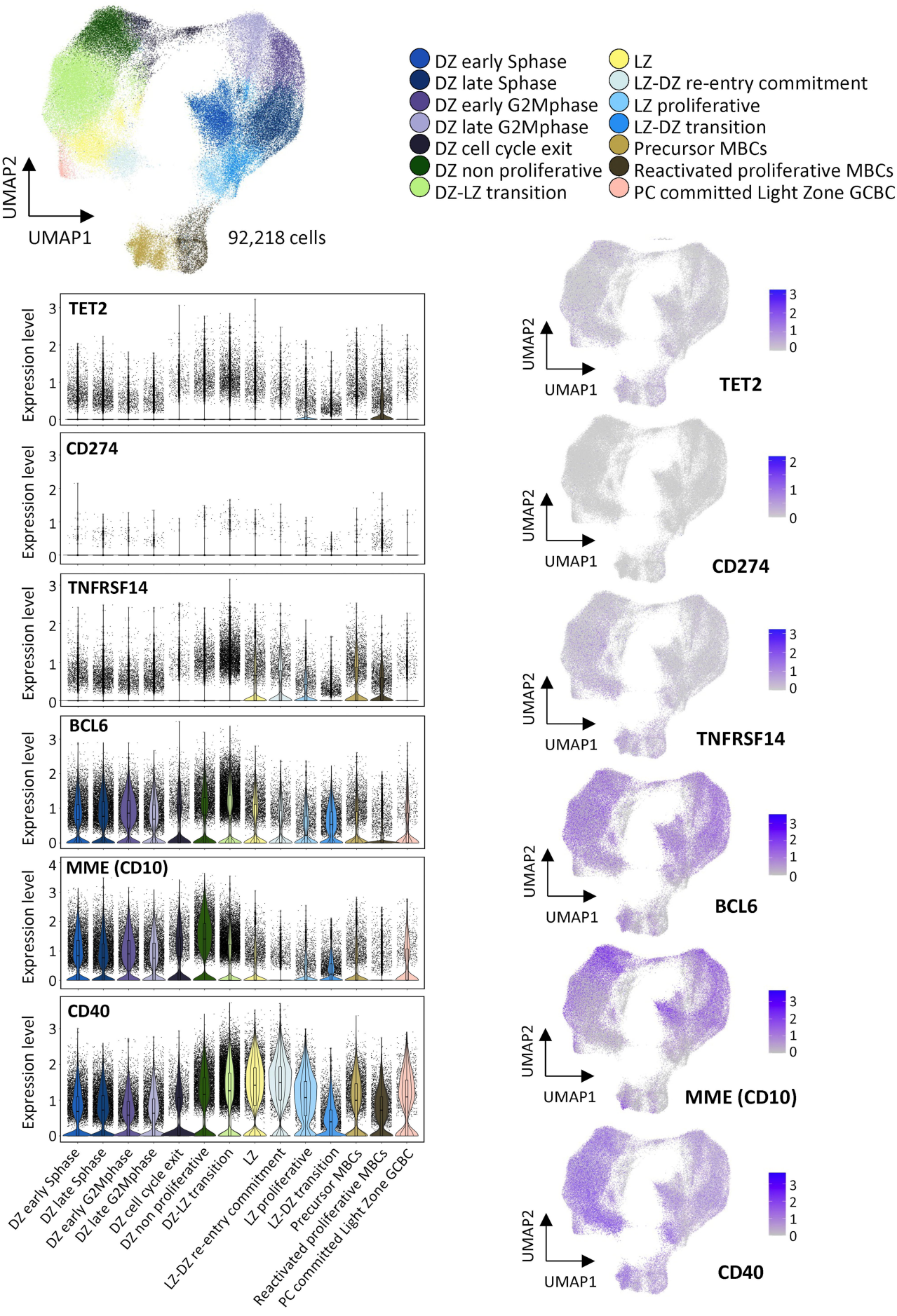
UMAP2
UMAP1
92,218 cells
DZ early Sphase
DZ late Sphase
DZ early G2Mphase
DZ late G2Mphase
DZ cell cycle exit
DZ non proliferative
DZ-LZ transition
LZ
LZ-DZ re-entry commitment
LZ proliferative
LZ-DZ transition
Precursor MBCs
Reactivated proliferative MBCs
PC committed Light Zone GCBC
TET2
CD274
TNFRSF14
BCL6
MME (CD10)
CD40
Expression level
DZ early Sphase
DZ late Sphase
DZ early G2Mphase
DZ late G2Mphase
DZ cell cycle exit
DZ non proliferative
DZ-LZ transition
LZ
LZ-DZ re-entry commitment
LZ proliferative
LZ-DZ transition
Precursor MBCs
Reactivated proliferative MBCs
PC committed Light Zone GCBC

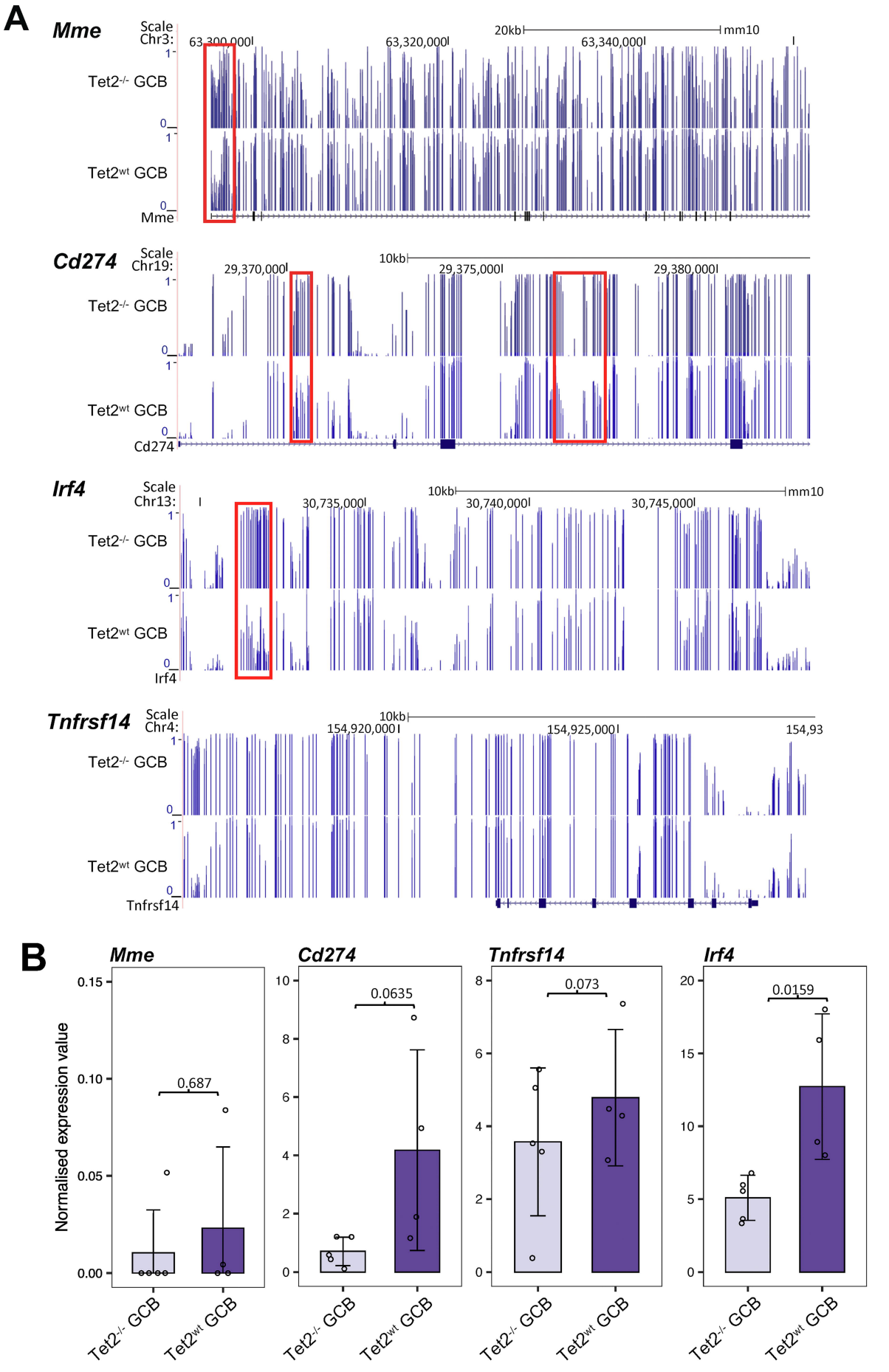
A
Mme
Scale
Chr3:
63,300,000
63,320,000
20kb
63,340,000
mm10
Tet2-/- GCB
Tet2wt GCB
Mme
Cd274
Chr19:
29,370,000
10kb
29,375,000
29,380,000
Cd274
Irf4
Chr13:
30,735,000
30,740,000
30,745,000
Tnfrsf14
Chr4:
154,920,000
154,925,000
154,93
B
Normalised expression value
0.687
0.0635
0.073
0.0159
Tet2-/- GCB
Tet2wt GCB

**SUPPLEMENTARY MATERIALS**

**SUPPLEMENTARY METHODS**

**Detection of *BCL6* rearrangements by capture-based sequencing**

Two cases (FL-09 and FL-16) were analysed using a bespoke capture panel designed to target genomic regions encompassing and flanking *BCL6* and the immunoglobulin loci (*IGH*, *IGK* and *IGL*), enabling detection of *BCL6* rearrangements (Supplementary Table 3).

Library preparation and target enrichment were performed similarly as described in the targeted next-generation sequencing section for mutation analysis. Briefly, 100 ng of FFPE-derived DNA was fragmented by Covaris ultrasonication, indexed using xGen™ UDI-UMI adapters (IDT), and enriched using the custom translocation capture probes. Enriched libraries were PCR-amplified and sequenced using 2 × 150 bp paired-end reads on an Illumina Novaseq X 25B platform. Read alignment and processing were performed using the same bioinformatic pipeline applied to the mutation panel.

Chromosomal translocations were identified using a combination of three structural variant callers: GRIDDS[1], Manta[2] and Delly[3]. Only on-target translocations supported by more than five split reads and assigned a “PASS” quality status were retained for downstream analysis. All candidate translocations were subsequently reviewed manually using the Integrative Genomics Viewer (IGV)[4].

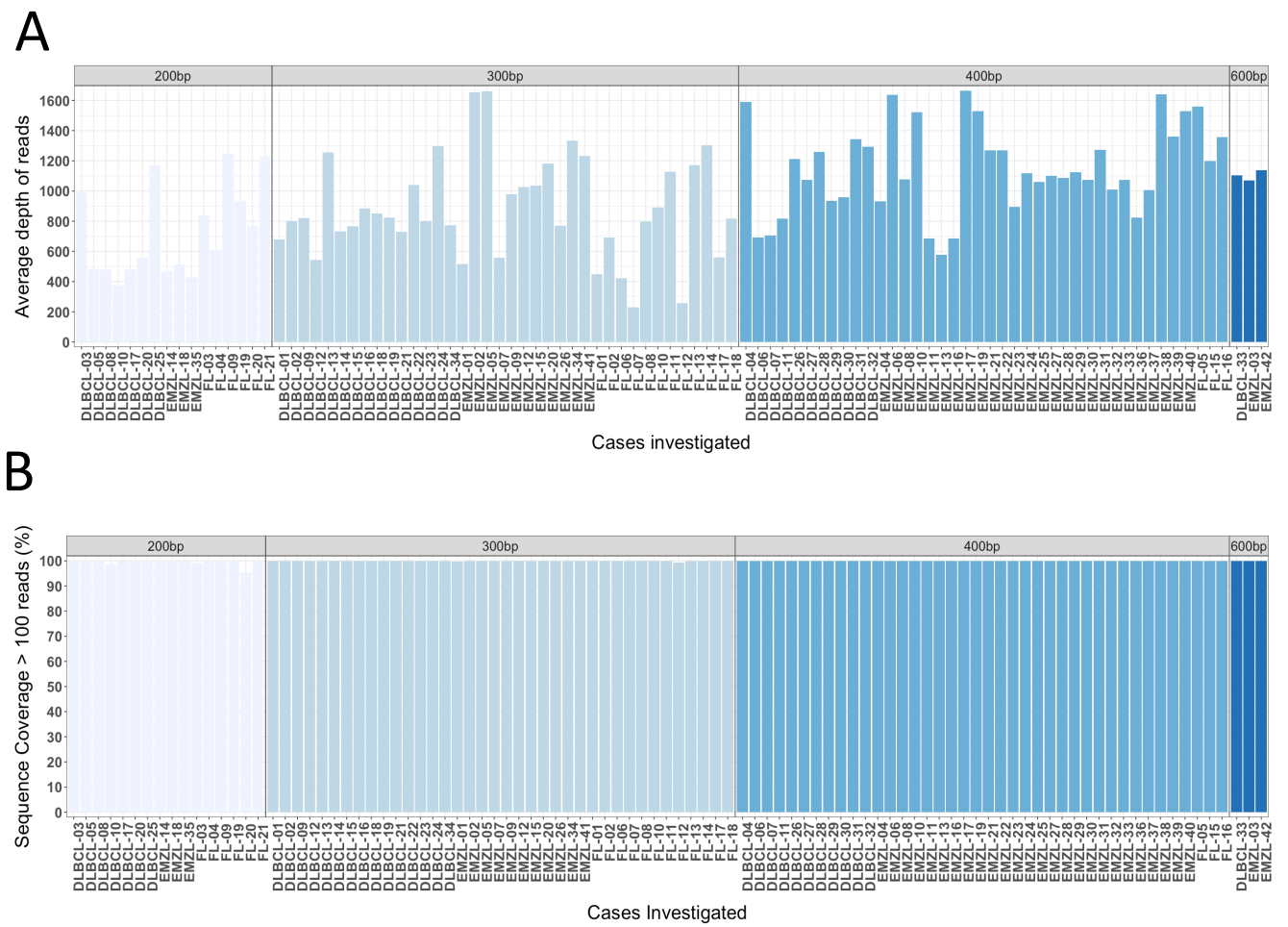


**Supplementary Figure S1.** Sequencing coverage of targeted NGS. DNA quality as measured by PCR of variable-sized genomic fragments is indicated on top of each panel. All cases with DNA quality only amenable for PCR amplification up to 300bp were investigated in duplicates.

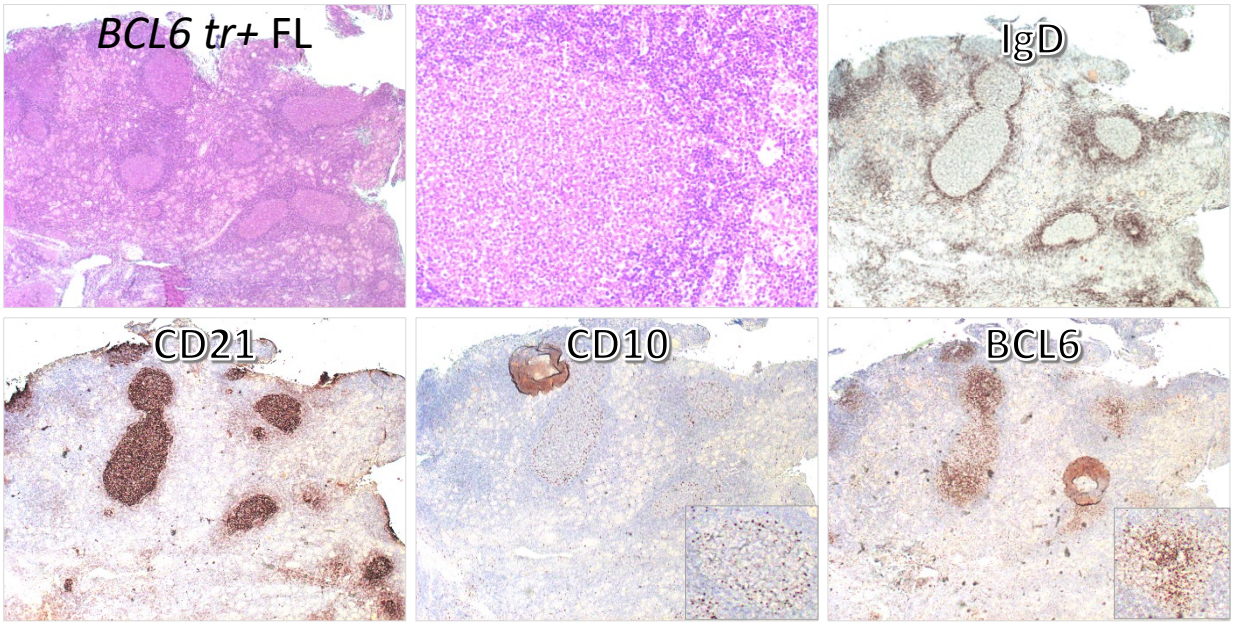


**Supplementary Figure S2.** Histopathology of a primary thyroid FL with *BCL6* translocation . The case (FL-11) displays follicular growth pattern with little involvement of the interfollicular region. The neoplastic B cells are CD10 negative but express BCL6.

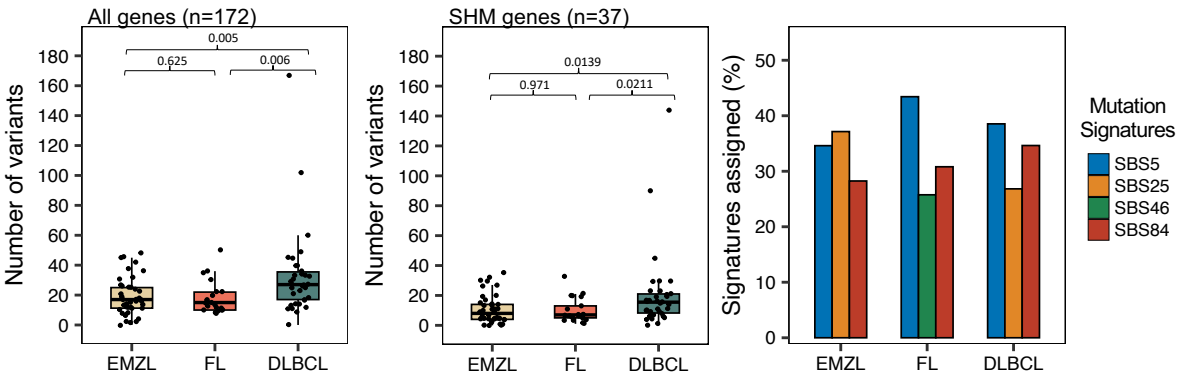


**Supplementary Figure S3**. Comparison of mutation load and signature among thyroid EMZL, FL and DLBCL. For mutation load analysis, all somatic variants (synonymous, non-synonymous, indels and changes in UTRs) are included, while for mutation signature analysis, only somatic single nucleotide changes are used. SHM: somatic hypermutation; SBS: single base substitutions.

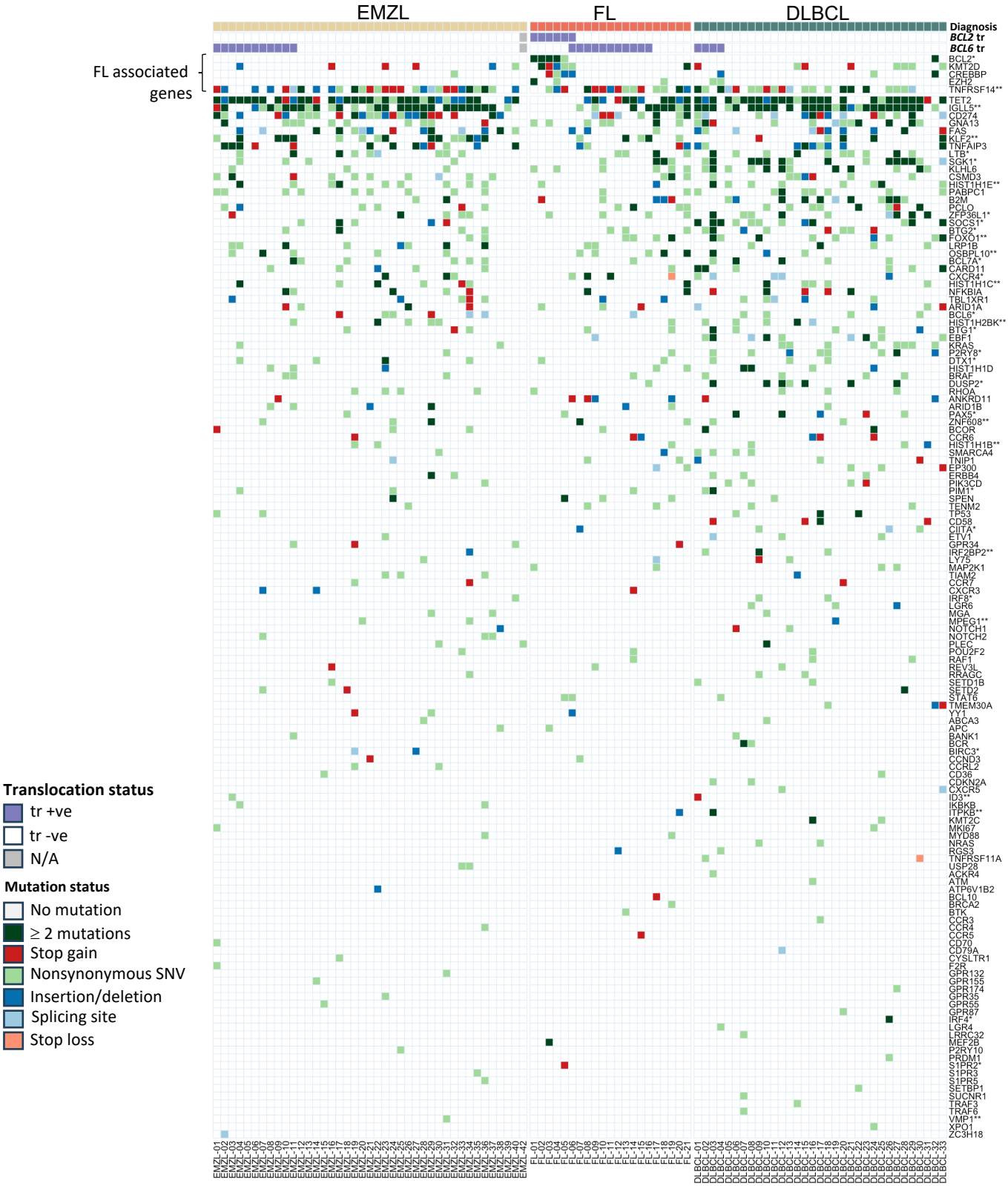


**Supplementary Figure S4.** Heatmap presentation of all potentially pathogenic mutations identified in in all three lymphoma entities. The mutated genes are grouped according to their association with lymphoma entity and ordered according to frequency. * and ** denote known and predicted somatic hypermutation targets respectively. FL: follicular lymphoma; DLBCL: diffuse large B-cell lymphoma; EMZL: extranodal marginal zone lymphoma of mucosa-associated lymphoid tissue; tr+ve: translocation positive, tr-ve: translocation negative; SNV: single nucleotide variation; SHM: somatic hypermutation.

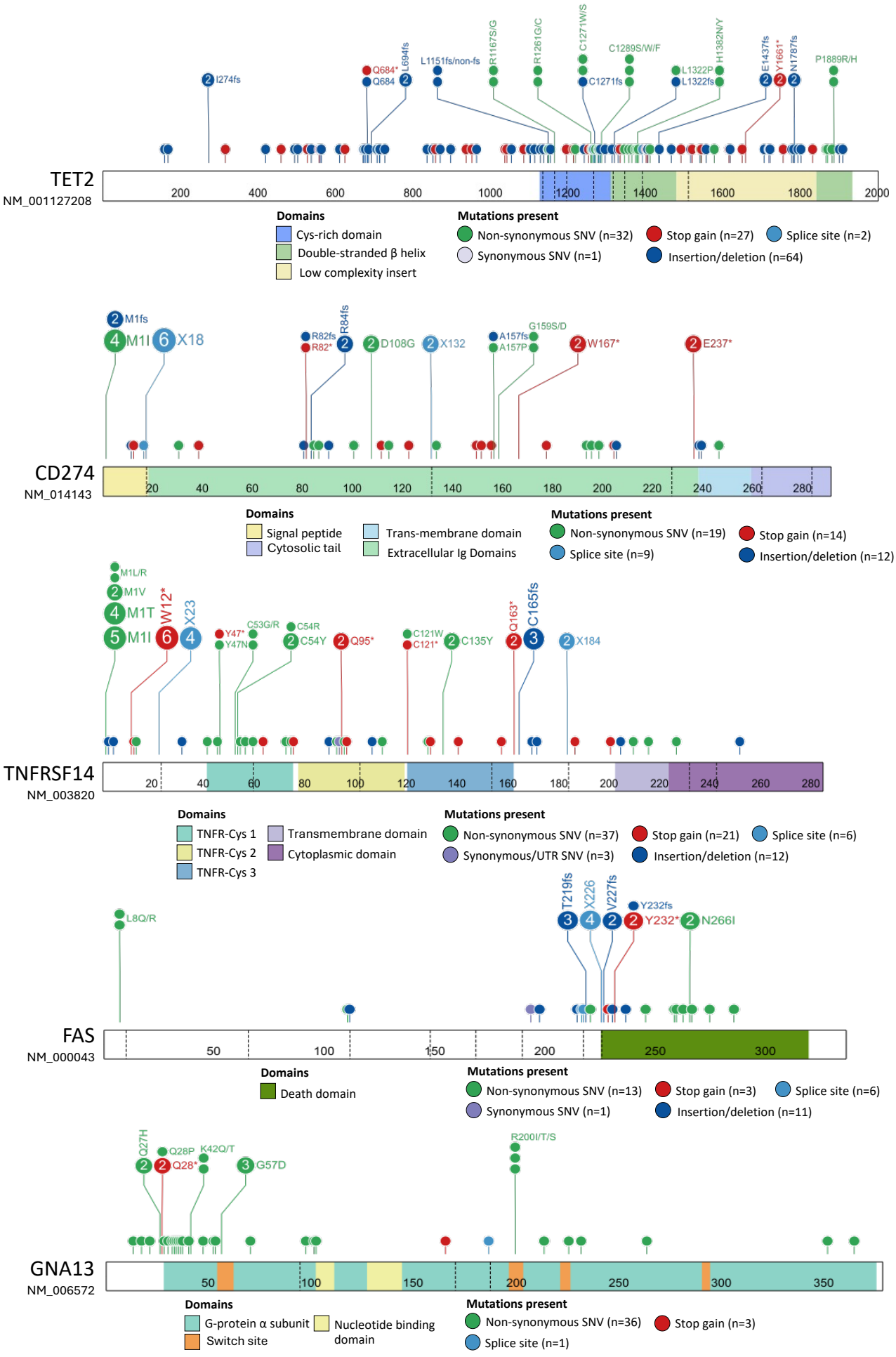


**Figure S5**: continue to the next page

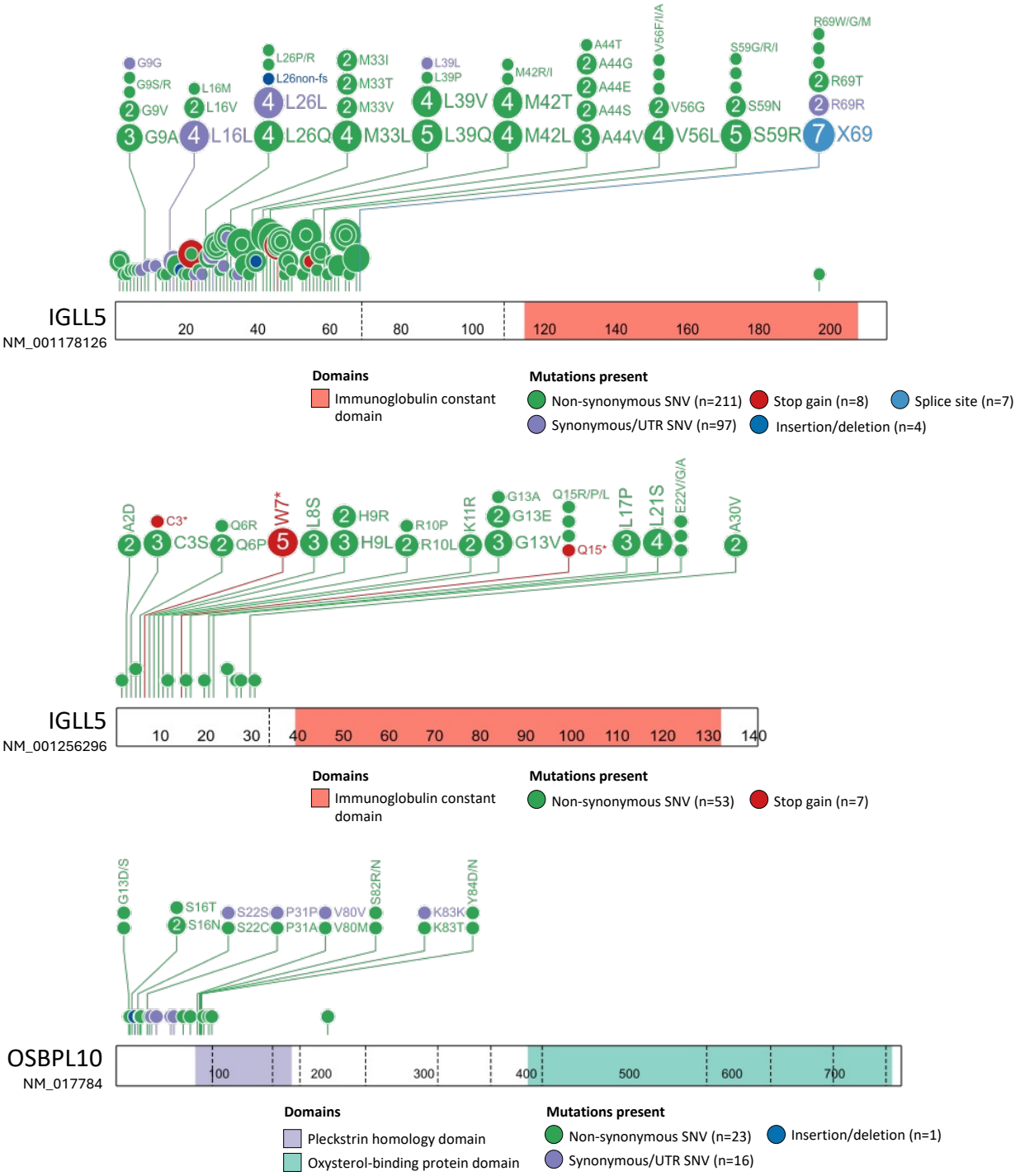


**Supplementary Figure S5.** Characteristics and distribution of mutations identified in genes frequently mutated in thyroid EMZL, DLBCL and *BCL2* translocation negative FL.

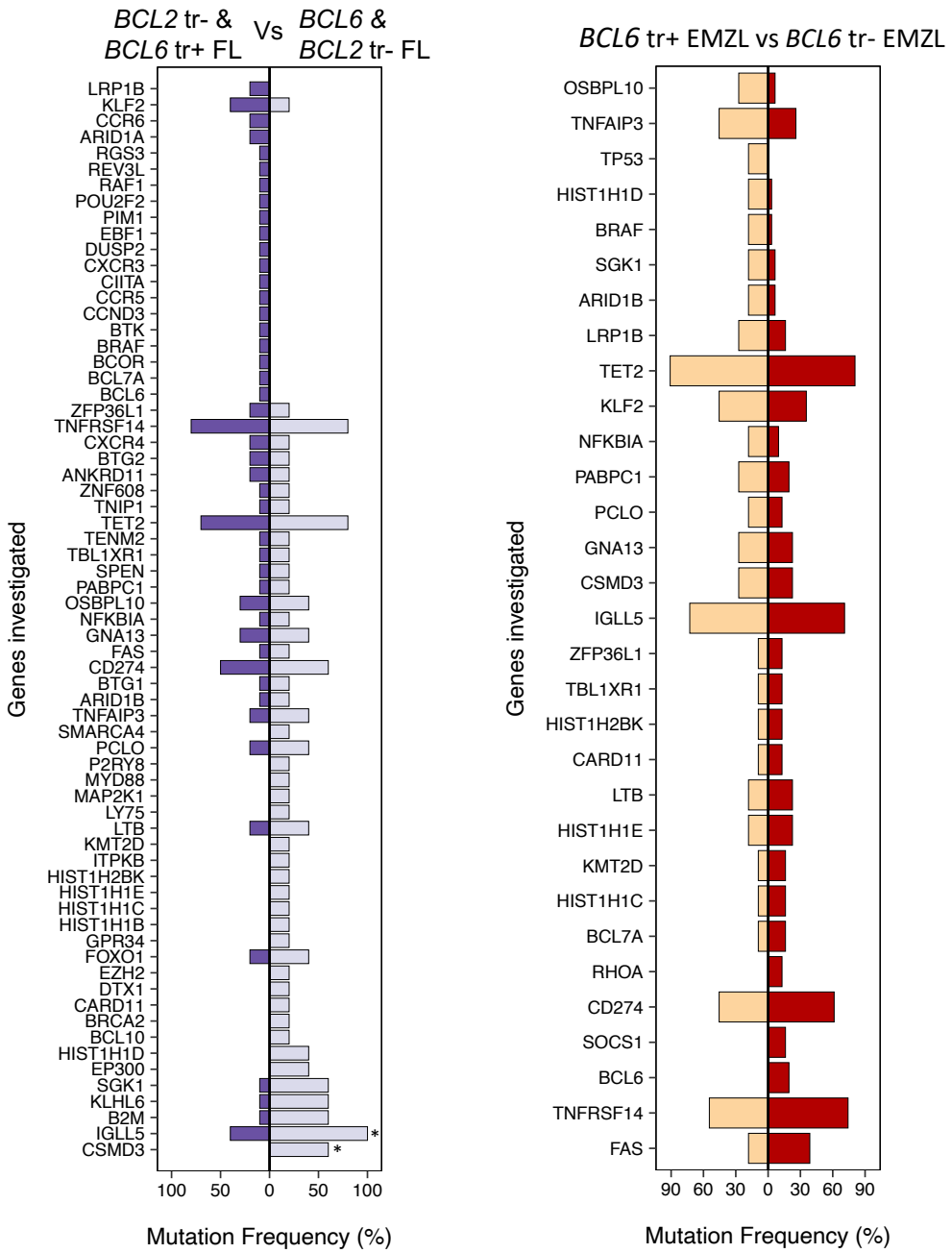


**Supplementary Figure S6.** Comparison of mutation frequency between subsets of thyroid EMZL and FL as indicated. FL: follicular lymphoma; EMZL: extranodal marginal zone lymphoma of mucosa-associated lymphoid tissue; tr+ve: translocation positive, tr-ve: translocation negative. * denotes significant changes between subsets.

# Thyroid FL

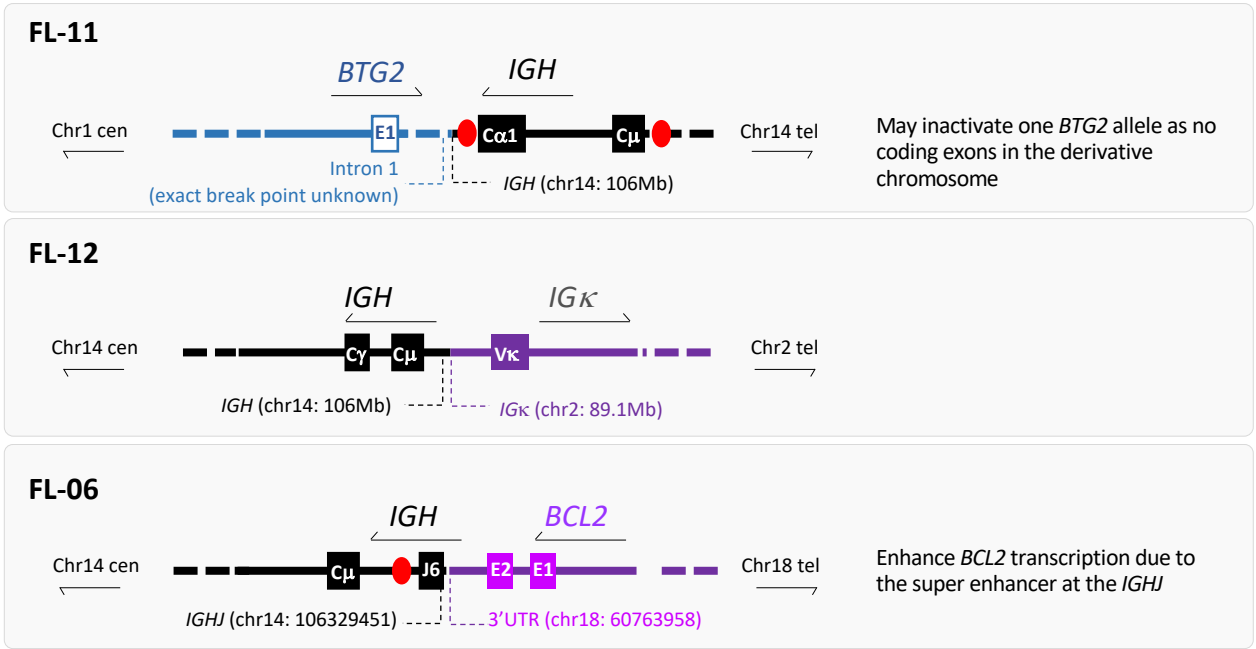


# Thyroid EMZL

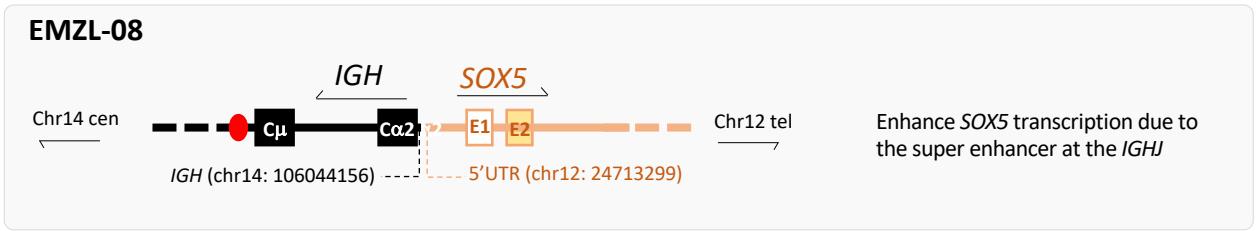


**Supplementary Figure S7.** Additional translocations detected in *BCL6* translocation positive thyroid FL and EMZL by targeted locus capture-based next generation sequencing (TLC-NGS). The sequence annotations are based on human genome (hg19) together with *IGH* super enhancers according to to Mikulasova et al [5]. FL: follicular lymphoma; EMZL: extranodal marginal zone lymphoma of mucosa-associated lymphoid tissue; cen: centromeric; tel: telomeric.

**SUPPLEMENTARY TABLES** see Supplementary Excel File

**Supplementary Table S1.** Antibodies and DNA probes used for immunohistochemistry and FISH respectively.

**Supplementary Table S2.** List of the genes investigated by TWIST capture and NGS.

**Supplementary Table S3:** List of the genes and coordinates investigated by TWIST capture translocation panel and NGS.

**Supplementary Table S4.** Clinical and laboratory features of thyroid lymphoma cohort

**Supplementary Table S5.** Variants detected by 172-gene panel next generation sequencing.

**REFERENCES**


1. Cameron DL, Baber J, Shale C, *et al.* GRIDSS2: comprehensive characterisation of somatic structural variation using single breakend variants and structural variant phasing. *Genome Biology.* 2021;22(1):202.
2. Chen X, Schulz-Trieglaff O, Shaw R, et al. Manta: rapid detection of structural variants and indels for germline and cancer sequencing applications. *Bioinformatics.* 2016;32(8):1220-1222.
3. Rausch T, Zichner T, Schlattl A, Stütz AM, Benes V, Korbel JO. DELLY: structural variant discovery by integrated paired-end and split-read analysis. Bioinformatics. 2012;28(18):i333-i339.
4. Thorvaldsdóttir, H., Robinson, J. T. & Mesirov, J. P. Integrative Genomics Viewer (IGV): high-performance genomics data visualization and exploration. *Brief Bioinform*. 2013;14(2):178–92.
5. Mikulasova A, Kent D, Trevisan-Herraz M, et al. Epigenomic translocation of H3K4me3 broad domains over oncogenes following hijacking of super-enhancers. Genome Res. 2022;32(7):1343–1354.